nature immunology

ARTICLES

https://doi.org/10.1038/s41590-019-0496-9

Locally instructed CXCR4^{hi} neutrophils trigger environment-driven allergic asthma through the release of neutrophil extracellular traps

Coraline Radermecker[1,2,3,9], Catherine Sabatel[1,3,9], Céline Vanwinge[4], Cecilia Ruscitti[2,3], Pauline Maréchal[2,3], Fabienne Perin[4], Joey Schyns[1,2,3], Natacha Rocks[4], Marie Toussaint[5,6], Didier Cataldo[4], Sebastian L Johnston[5,6,7], Fabrice Bureau[1,3,8,10*] and Thomas Marichal[1,2,3,8,10*]

Low exposure to microbial products, respiratory viral infections and air pollution are major risk factors for allergic asthma, yet the mechanistic links between such conditions and host susceptibility to type 2 allergic disorders remain unclear. Through the use of single-cell RNA sequencing, we characterized lung neutrophils in mice exposed to a pro-allergic low dose of lipopolysaccharide (LPS) or a protective high dose of LPS before exposure to house dust mites. Unlike exposure to a high dose of LPS, exposure to a low dose of LPS instructed recruited neutrophils to upregulate their expression of the chemokine receptor CXCR4 and to release neutrophil extracellular traps. Low-dose LPS–induced neutrophils and neutrophil extracellular traps potentiated the uptake of house dust mites by CD11b^{+}Ly-6C^{+} dendritic cells and type 2 allergic airway inflammation in response to house dust mites. Neutrophil extracellular traps derived from CXCR4^{hi} neutrophils were also needed to mediate allergic asthma triggered by infection with influenza virus or exposure to ozone. Our study indicates that apparently unrelated environmental risk factors can shape recruited lung neutrophils to promote the initiation of allergic asthma.

Exposure to naturally occurring aeroallergens such as house dust mites (HDM), pollens or animal dander can, in some predisposed individuals, lead to allergic sensitization and the development of allergic asthma, a major public-health problem with high socio-economic impacts[1,2]. While genome-wide studies have discovered genetic polymorphisms associated with allergic susceptibility[3], the worldwide increase in the prevalence of allergies over the last decades points towards a major contribution of the environment[4,5]. Epidemiological studies have identified environmental risk factors for allergic asthma, including respiratory viral infections[6], air pollutants[7] or urban lifestyles associated with decreased exposure to microbes or their products such as bacterial endotoxins (LPS)[8,9]. A better understanding of the mechanisms by which pro-allergic environmental conditions shape the lung immune system to initiate allergic airway responses is an unmet and urgent need that may open novel therapeutic avenues for allergic asthma.

Allergic airway inflammation, a cardinal feature of allergic asthma, is thought to result from an aberrant type 2 immune response directed against inhaled allergens[10,11]. The initiation of type 2 immunity to HDM, a major allergen source in humans[12], involves sensing of LPS and HDM compounds by epithelial cells and the release of pro-allergic alarmins that instruct lung dendritic cells (DCs) to sample allergens, transport them to the draining lymph node (LN) and induce allergen-specific CD4^{+} type 2 helper T cells (T_H2 cells). On subsequent HDM challenge, T_H2 effector cells secrete type 2 cytokines such as IL-4, IL-5 and IL-13, which orchestrate features of allergic airway inflammation, including airway eosinophilia and goblet cell metaplasia through IL-5- and IL-13-dependent mechanisms, respectively[11,13].

Neutrophils are known to function as first responders specialized in pathogen clearance and as prototypic effector cells of type 17 responses. However, new evidence points to the complexity and functional diversity of neutrophils[14,15]. The role of neutrophils in asthma has mainly been investigated in severe asthma, which is characterized by a type 17-mediated neutrophilic inflammation[16–19]. In type 2 allergic asthma, the role of neutrophils has been investigated in the effector phase but not the initiation phase of type 2 responses[17,20]. Indeed, neutrophil-derived DNA found in neutrophil extracellular traps (NETs), which also contain modified histone proteins such as citrullinated histone H3 (Cit-H3) and granule proteins such as neutrophil elastase (NE) and myeloperoxidase (MPO)[15], contributed to the manifestations of rhinovirus-induced allergic asthma exacerbations[20].

Here, using single-cell RNA sequencing (scRNA-seq) and mouse models of allergic asthma triggered by three distinct pro-allergic environmental factors, we found that locally programmed, NET-releasing CXCR4^{hi} lung neutrophils acted as early triggers of type 2 allergic airway inflammation. Our results indicate that phenotypically and functionally distinct tissue neutrophils act as common determinants of environment-driven allergic asthma onset in mice.

Results

Low-dose LPS exposure potentiates HDM-induced allergic asthma. To investigate the mechanisms of environment-driven

[1]Laboratory of Cellular and Molecular Immunology, GIGA Institute, Liege University, Liege, Belgium. [2]Laboratory of Immunophysiology, GIGA Institute, Liege University, Liege, Belgium. [3]Faculty of Veterinary Medicine, Liege University, Liege, Belgium. [4]Laboratory of Tumor and Development Biology, GIGA Institute, Liege University, Liege, Belgium. [5]Airway Disease Section, National Heart and Lung Institute, Imperial College London, London, UK. [6]Medical Research Council and Asthma UK Centre in Allergic Mechanisms of Asthma, London, UK. [7]Imperial College Healthcare National Health Service Trust, London, UK. [8]Walloon Excellence in Life Sciences and Biotechnology, Wallonia, Belgium. [9]These authors contributed equally: Coraline Radermecker, Catherine Sabatel. [10]These authors jointly supervised this work: Fabrice Bureau, Thomas Marichal. *e-mail: fabrice.bureau@uliege.be; t.marichal@uliege.be

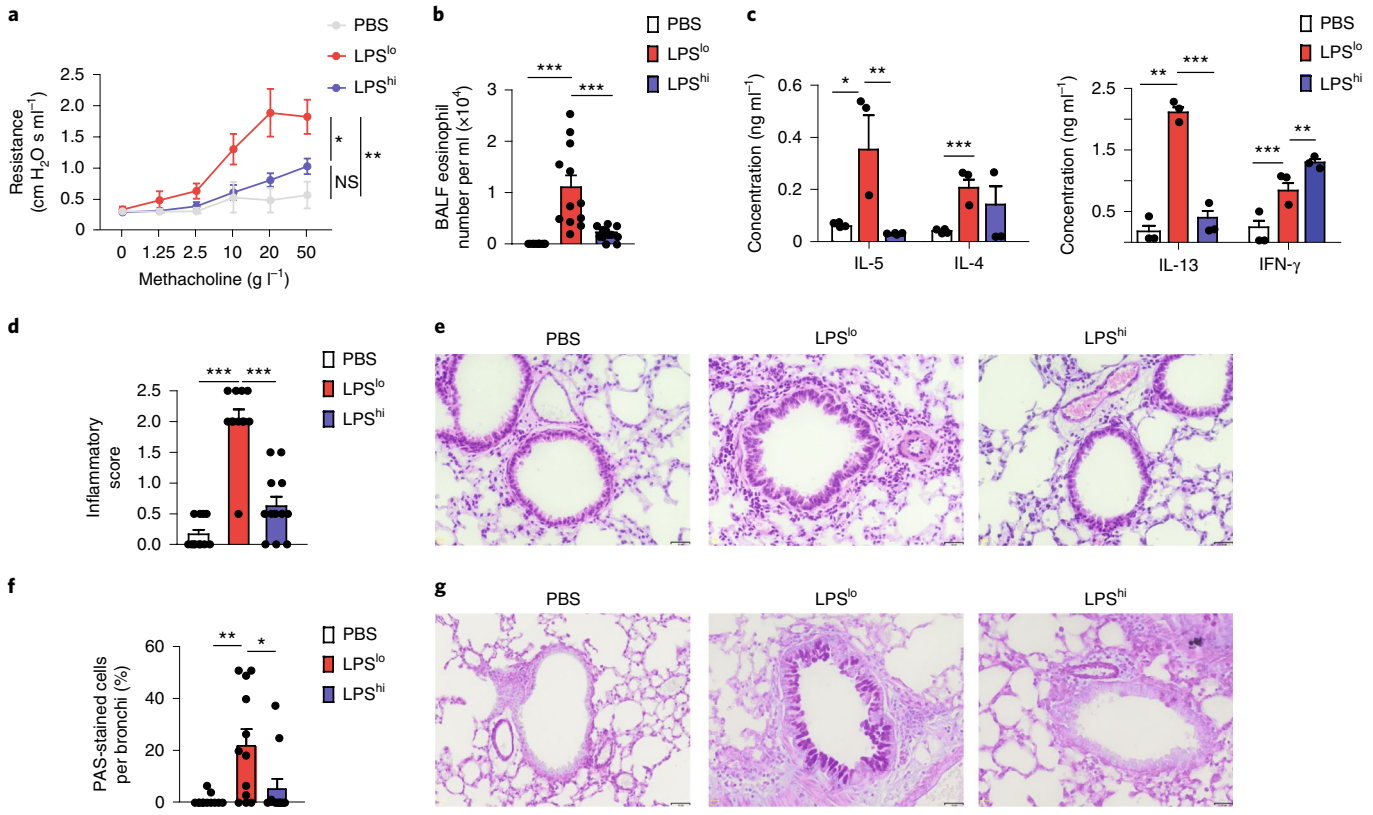


Fig. 1 | Pre-exposure to low-dose LPS potentiates HDM-induced type 2 allergic asthma. a, Invasive measurement of dynamic airway resistance on methacholine inhalation showing bronchial hyperreactivity in vehicle-HDM, LPS^{lo}-HDM and LPS^{hi}-HDM mice, assessed 3 d after the second HDM administration. **b**, Eosinophil cell counts in the BALF of mice, as in **a**. **c**, Enzyme-linked immunosorbent assay (ELISA) measurement of cytokine production by HDM-restimulated bronchial LN (BLN) cells of mice, as in **a**. **d**, Inflammatory score estimating perivascular and peribronchial inflammation, quantified from H&E-stained lung sections of mice, as in **a**. **e**, Representative hematoxylin and eosin (H&E) staining of lung sections of mice as in **a**. **f**, Quantification of PAS-stained epithelial cells per bronchi showing airway mucus production in mice, as in **a**. **g**, Representative PAS staining of lung sections of mice, as in **a**. **a**–**d**,**f**, Data show mean + s.e.m. and are pooled from 2 independent experiments ($n = 6$ mice per group) (**a**) or ≥3 independent experiments (**b**–**d**,**f**), each symbol representing individual mice (**b**,**d**,**f**) ($n = 12$ per group) or independent experiments in which cells from 4 mice were pooled by group (**c**). *P* values were calculated using a mixed-effects model with Geisser greenhouse correction (**a**) or a one-way analysis of variance (ANOVA) with Tukey's post hoc test (**b**–**d**,**f**). $^*P < 0.05$; $^{**}P < 0.01$; $^{***}P < 0.001$. NS, not significant. Scale bar, 32 µm.

initiation of allergic asthma in mice, we used a model of exposure to HDM in mice pre-exposed to a pro-allergic environmental factor, namely a low dose of LPS[21]. Different doses of LPS, ranging from 0.1 ng to 10 µg, were administered intranasally (i.n.) to groups of BALB/c mice, which were exposed 1 and 8 d later to 40 and 10 µg of HDM i.n., respectively. At day 11, airway eosinophilia, a feature of type 2 allergic asthma[11], was virtually absent in vehicle pre-exposed HDM-treated mice, but it reached a peak in mice pre-exposed to 100 ng of LPS and returned to baseline with 10 µg of LPS (Supplementary Fig. 1a,b). Single exposures to either 100 ng or 10 µg of LPS were chosen to model a pro-allergic, 'hygienic' (LPS^{lo}) or a protective[22], 'nonhygienic' (LPS^{hi}) environment, respectively. LPS^{lo} mice treated with HDM (LPS^{lo}-HDM mice) developed features of allergic asthma 3 d after the second HDM instillation, including increased bronchial hyperreactivity to methacholine (Fig. 1a), airway eosinophilia (Fig. 1b), a higher secretion of IL-4, IL-5 and IL-13 by total LN cells restimulated with HDM (Fig. 1c), perivascular and peribronchial leukocyte infiltration (Fig. 1d,e), and increased bronchial mucus production (Fig. 1f,g) when compared to vehicle-HDM or LPS^{hi}-HDM mice. Of note, CD45$^+$CD11b^{hi}Ly-6G^{hi} neutrophils, quantified by flow cytometry, were massively recruited into the lungs of LPS^{lo} and LPS^{hi} mice between 6 and 24 h after LPS exposure (Supplementary Fig. 1c,d). Thus, low-dose exposure to LPS induced a lung environment that promoted type 2 immunity to HDM and the development of allergic asthma.

scRNA-seq identifies particular neutrophils in LPS^{lo} mice. To investigate the transcriptional diversity of lung neutrophils, we performed scRNA-seq. Twenty-four hours after vehicle, LPS^{lo} and LPS^{hi} i.n., neutrophils were first enriched from lung single-cell suspensions pooled from 3 BALB/c mice per condition by negative selection with MACS and were then FACS sorted as CD45$^+$ cells (Supplementary Fig. 2a–c). With the 10x Genomics platform[23], cells were subjected to single-cell droplet encapsulation, scRNA-seq and quality-control filtering (Supplementary Fig. 2d,e). A total of 1,406, 2,146 and 2,746 cells were analyzed in vehicle, LPS^{lo} and LPS^{hi} mice, respectively. Nonlinear dimensional reduction and graph-based clustering of single cells pooled from vehicle, LPS^{lo} and LPS^{hi} mice identified 6 transcriptionally distinct clusters of neutrophils, all characterized by high expression of *S100a8*, *S100a9* and *Csf3r* transcripts (cluster 0 through cluster 5; Fig. 2a and Supplementary Fig. 2f,g). Neutrophils from vehicle lungs were grouped in one cluster (cluster 0; Fig. 2b–d and Supplementary Fig. 3a–d), while neutrophils from LPS^{lo} and LPS^{hi} mice were segregated into five additional clusters (clusters 1–5, Fig. 2b–d). Neutrophils in cluster 1 were almost uniquely found in lungs from LPS^{lo} mice, while neutrophils in clusters 2, 3 and 5 were nearly exclusively present in lungs from LPS^{hi} mice, and neutrophils in cluster 4 were equally distributed between LPS^{hi} and LPS^{lo} mice (Fig. 2b–d). We performed a differential expression analysis, and we defined a common,

dose-independent, LPS-induced signature as the list of transcripts that were commonly upregulated in each of the clusters 1 to 5 as compared to cluster 0 (Supplementary Fig. 3e,f). We then identified LPS^{lo} or LPS^{hi} signatures as the lists of transcripts that were upregulated in cluster 1 or clusters 2, 3 and 5, respectively, as compared to cluster 0, and that were absent from the common LPS signature. *Cxcr4* and *Lamp-1* transcripts, which code for proteins detectable by flow cytometry, were significantly upregulated in LPS^{lo} neutrophils as compared to LPS^{hi} neutrophils (Fig. 2e). The LPS^{hi} signature comprised 25 transcripts that were enriched in processes such as complement receptor-mediated signaling pathways (*Fpr1, Fpr2*) and response to type 1 or type 2 interferon (IFN) (*Ifitm1, Ifitm3, Ifi47*) based on Gene Ontology analysis (Fig. 2e–g). The LPS^{lo} signature contained 97 transcripts that were enriched in genes involved in endoplasmic reticulum stress (*Atf3, Atf4, Bax*), reactive oxygen species synthesis (*Ptgs2, Arg2, Il1b*), oxidative stress (*Rps3, Prdx6, Jun*) and ERK1/2 signaling cascade (*Cd74, C3, Hmgb1*) (Fig. 2e,f,h), responses that have all been implicated in the formation and release of NETs[15,24]. Thus, lung neutrophils induced by a pro-allergic, low dose of LPS are transcriptionally distinct from those induced by a high LPS dose.

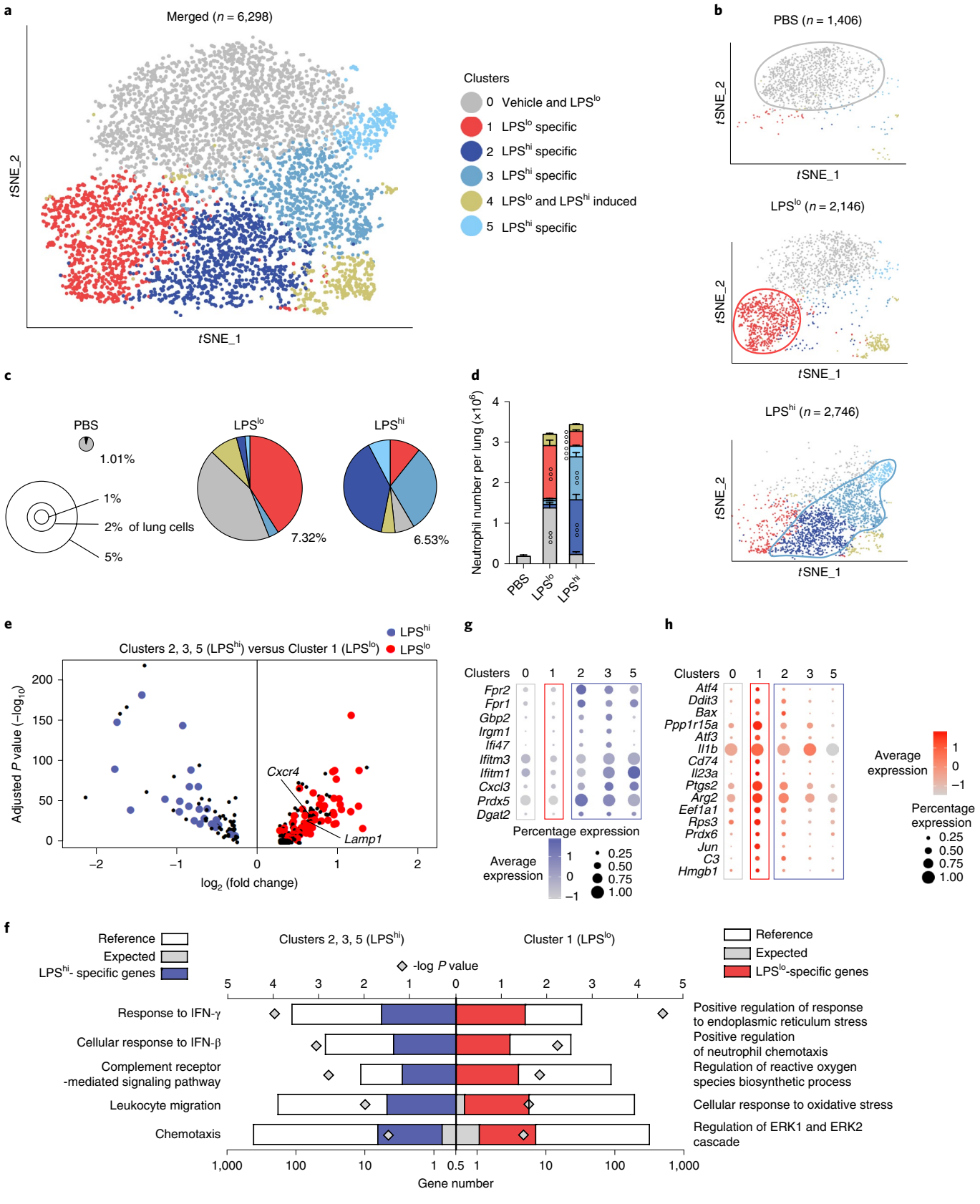
LPS^{lo} locally triggers NET-releasing CXCR4^{hi} neutrophils. To validate the scRNA-seq findings and identify the neutrophils induced by LPS^{lo} treatment in vivo, we exposed BALB/c mice to vehicle, LPS^{lo} or LPS^{hi} treatment and assessed the expression of CXCR4 and Lamp-1 on lung CD45^{+}CD11b^{hi}Ly-6G^{hi} neutrophils 24 h later. We found a significant upregulation of CXCR4 and Lamp-1 on lung neutrophils from LPS^{lo} mice as compared to neutrophils from vehicle or LPS^{hi} mice (Fig. 3a,b). The expression of CD49d, an integrin reported to be highly expressed on CXCR4^{hi} blood neutrophils[25], was also upregulated on lung neutrophils from LPS^{lo} mice (Fig. 3a,b). Next, we performed time-course analyses of CXCR4 expression on bone marrow (BM), blood and lung CD45^{+}CD11b^{hi}Ly-6G^{hi} neutrophils isolated 6, 12, 18, 24 and 48 h after treatment in vehicle, LPS^{lo} and LPS^{hi} mice. In the lung, CXCR4 expression on CD45^{+}CD11b^{hi}Ly-6G^{hi} neutrophils started to increase 18 h after LPS^{lo}, reached a peak at 24 h and returned to baseline after 48 h (Fig. 3c). Expression of CXCR4 on lung CD45^{+}CD11b^{hi}Ly-6G^{hi} neutrophils from LPS^{hi} mice was similar to that of vehicle mice (Fig. 3c). Of note, while we detected a rhythmic oscillation in the expression of CXCR4 on blood neutrophils[26], the oscillation was not affected by treatment with LPS, regardless of the dose (Fig. 3c). Expression of CXCR4 on BM CD45^{+}CD11b^{hi}Ly-6G^{hi} neutrophils was similar in LPS^{lo} and vehicle mice (Fig. 3c), indicating that low-dose LPS administered i.n. instructs the neutrophils locally and not at distant sites. Morphologically, CXCR4^{hi}CD49d^{hi} neutrophils sorted from the lungs of LPS^{lo} mice were smaller and displayed a higher nucleus/cytoplasm ratio and a hypersegmented nucleus compared to lung CXCR4^{lo}CD49d^{lo} neutrophils from LPS^{hi} mice (Fig. 3d and Supplementary Fig. 4a–d).

Lung CXCR4^{hi}CD49d^{hi} neutrophils sorted from LPS^{lo} mice released NETs ex vivo, while lung CXCR4^{lo}CD49d^{lo} neutrophils from vehicle or LPS^{hi} mice did not (Fig. 3e and Supplementary Fig. 4e–g). In addition, the amount of free double-stranded DNA (dsDNA) and of NE–DNA complexes, which are characteristic of NETs[15], were higher in the bronchoalveolar lavage fluid (BALF) of LPS^{lo} mice 24 h after LPS than in the vehicle and LPS^{hi} mice (Fig. 3f,g), while the amounts of Cit-H3, a modified form of histone H3 implicated in chromatin decondensation and NET formation[15], were specifically increased in the lungs of LPS^{lo} mice (Fig. 3h,i). High-resolution confocal microscopy indicated the presence of extracellular MPO^{+}Cit-H3^{+} NETs in the lungs of LPS^{lo} mice, unlike in vehicle or LPS^{hi} mice (Fig. 3j,k). Notably, neutrophil depletion with an antibody against Ly-6G was associated with an absence of NETs 24 h after LPS in the lungs of anti-Ly-6G-treated LPS^{lo} mice (Supplementary Fig. 5), indicating that NETs were exclusively derived from neutrophils. Concordant with the upregulation of CXCR4, NETs were detected at 18 h after low-dose LPS, but not detected after 48 h (Supplementary Fig. 6a,b). These observations indicate that neutrophils recruited to the lungs of LPS^{lo} mice had a CXCR4^{hi}CD49d^{hi}Lamp-1^{hi} phenotype that was only detected in the lungs, and were prone to release NETs, while lung neutrophils recruited in LPS^{hi} mice were phenotypically similar to steady-state neutrophils and did not release NETs.

CXCR4^{hi} neutrophils and NETs trigger allergic airway inflammation in LPS^{lo} mice. To address whether the effect of low-dose LPS on HDM-induced allergic airway inflammation was mediated by neutrophils, LPS^{lo}-HDM mice were administered Sch527123, an antagonist of the chemokine receptor CXCR2 (anti-CXCR2) (ref. [27]), orally 2 h before and 4 and 8 h after LPS^{lo}, and 2 h before and 4 h after i.n. administration of 40 µg of HDM, to inhibit the LPS-induced neutrophil recruitment to the lung[28]. Treatment with anti-CXCR2 significantly reduced numbers of lung CD45^{+}CD11b^{hi}Ly-6G^{hi} neutrophils 24 h after LPS treatment in LPS^{lo} mice (Fig. 4a,b). LPS^{lo}-HDM mice treated with anti-CXCR2 had significantly reduced airway eosinophilia (Fig. 4c), HDM-specific type 2 immune responses (Fig. 4d), perivascular and peribronchial inflammation (Fig. 4e,f) and mucus cell production (Fig. 4g,h) compared to vehicle LPS^{lo}-HDM mice. In a different approach, we isolated lung neutrophils from vehicle, LPS^{lo} or LPS^{hi} mice by MACS negative selection and FACS CD45^{+} sorting 24 h after LPS (vehicle, LPS^{lo} and LPS^{hi} neutrophils, respectively) and adoptively transferred 5×10^{5} neutrophils in the trachea of naive recipients together with 40 µg of HDM, which were exposed to 10 µg of HDM i.n. 7 d later and analyzed 11 d after transfer. Transfer of LPS^{lo} neutrophils was sufficient to trigger airway eosinophilia (Fig. 4i), HDM-specific type 2 immunity (Fig. 4j), peribronchial inflammation (Fig. 4k,l) and increased mucus production (Fig. 4m,n) in HDM-treated recipient mice, while all these features were significantly lower in mice that received vehicle or LPS^{hi} neutrophils.

Fig. 2 | ScRNA-seq analysis of the lung neutrophil compartment 24 h after pro-allergic low or protective high LPS exposure. a, *t*SNE plots depicting the transcriptional identity of lung neutrophils merged from vehicle, LPS^{lo} and LPS^{hi} mice 24 h after treatment, analyzed by scRNA-seq ($n=3$ pooled mice per group). **b**, *t*SNE plots depicting the transcriptional identity of lung neutrophils from the three separate experimental conditions, as in **a**. **c**, Pie charts depicting the relative contribution of each neutrophil cluster to the pool of neutrophils in lungs of mice, as in **a**. Insets indicate average percentage of neutrophils among total lung cells. **d**, Absolute numbers of lung neutrophils per cluster in mice, as in **a**. **e**, Volcano plot depicting the differentially expressed genes between LPS^{hi} and LPS^{lo} lung neutrophils of mice, as in **a**. Transcripts characteristic of the common LPS, the LPS^{lo}- and LPS^{hi}-specific signatures are colored in black, red and blue, respectively. **f**, PANTHER GO enrichment tests on the genes of the LPS^{hi} (left) and LPS^{lo} (right) signatures. **g**, **h**, Dot plots showing average expression of genes of the LPS^{hi} (**g**) and LPS^{lo} (**h**) signatures within neutrophil clusters. **d**, Data show mean + s.e.m. ($n=3$ mice per group). *P* values were calculated with a two-way ANOVA with Tukey's *post hoc* test (**d**), a likelihood ratio test based on zero-inflated data to identify positive and negative markers of a single cluster compared to some or all other clusters (**e**) or a two-tailed Mann–Whitney *U*-test with Benjamini–Hochberg false discovery rate (FDR) correction (**f**). The symbol ° within a given cluster in **d** indicates that neutrophil numbers in that cluster are significantly different from the ones of the same cluster in the two other experimental conditions. °°°$P<0.001$.

To test the contribution of NETs to the initiation of allergic airway inflammation in LPS^{lo}-HDM mice, we targeted the NETs with 4 daily intraperitoneal (i.p.) injections of DNase, which degrades NETs[20,29], starting 1 d before LPS^{lo} treatment, or with 8 i.p. injections of either the NE inhibitor GW-311616 (NEi)[15] or an inhibitor of the arginine deiminase PAD4 (Cl-amidine)[30], every 12 h starting 1 d before LPS^{lo} treatment. Treatments with DNase, NEi and Cl-amidine resulted in a significant decrease of



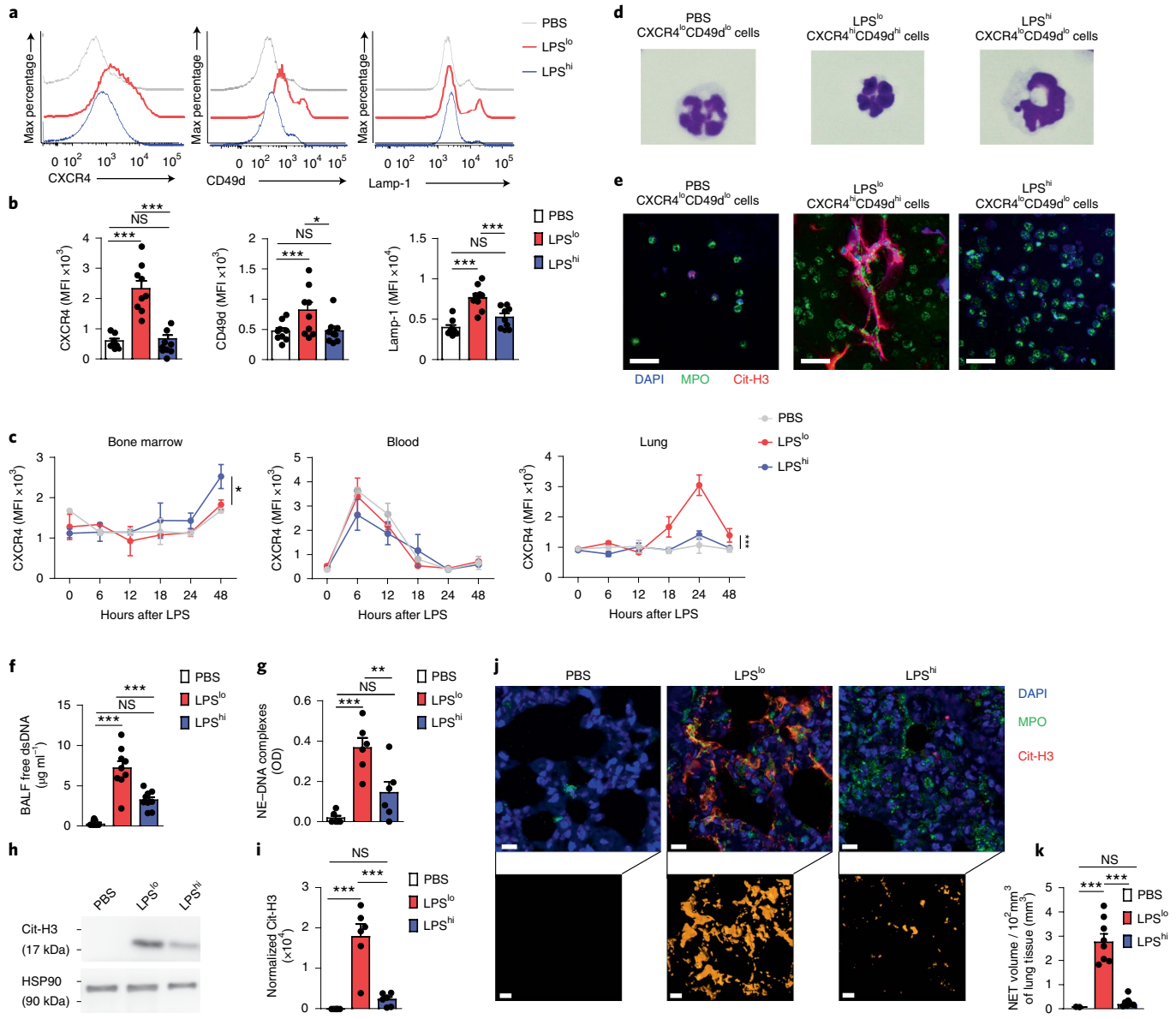


Fig. 3 | Pro-allergic low-dose LPS instructs lung neutrophils to upregulate CXCR4, CD49d and Lamp-1 and release NETs. a, Representative histograms of CXCR4, CD49d and Lamp-1 expression by lung CD45$^+$CD11b^{hi}Ly-6G^{hi} neutrophils from vehicle, LPS^{lo} and LPS^{hi} mice 24 h after treatment. **b**, MFI showing quantification of CXCR4, CD49d and Lamp-1 expression by lung CD45$^+$CD11b$^+$Ly-6G$^+$ neutrophils, as in **a**. **c**, Kinetic analysis of CXCR4 expression by bone marrow, blood and lung CD45$^+$CD11b^{hi}Ly-6G^{hi} neutrophils from mice, as in **a**. **d**, Representative photographs of FACS-sorted CXCR4^{lo}CD49d^{lo}, CXCR4^{lo}CD49d^{lo} and CXCR4^{hi}CD49d^{hi} lung neutrophils from mice, as in **a**. **e**, Confocal microscopy stainings of Cit-H3$^+$MPO$^+$DAPI$^+$ NETs released from ex vivo-cultured neutrophils, as in **d**. Pictures are representative of one of four independent sorting experiments. **f**, Levels of extracellular dsDNA in the BALF of vehicle, LPS^{lo} and LPS^{hi} mice 24 h after treatment. **g**, ELISA measurement of NE–DNA complexes in the BALF of mice, as in **f**. **h**, Representative blots of Cit-H3 and HSP90α (loading control) assessed by Western blot of lung protein extracts from mice, as in **f**. **i**, Quantification of normalized Cit-H3 levels in lung protein extracts of mice, as in **f**. **j**, Confocal microscopy stainings (top) and three-dimensional modeling (bottom) of Cit-H3$^+$MPO$^+$ NETs on lung sections of mice, as in **f**. Pictures are representative of one of more than 6 lungs analyzed. **k**, Quantification of NET volume in lung sections of mice, as in **f** ($n = 8$ mice per group). Data show mean + s.e.m and are pooled from 3 independent experiments (**b**,**f**,**g**,**i**) ($n = 9,9,6,6$ mice per group, respectively) or 2 independent experiments per time point analyzed (**c**) ($n = 3$ mice per time point). *P* values were calculated with a one-way ANOVA with Tukey's post hoc test. $^*P < 0.05$; $^{**}P < 0.01$; $^{***}P < 0.001$. *P* values compare LPS^{lo} versus vehicle or LPS^{hi} mice in **c** (that is, treatment effect). OD, optical density; NS, not significant. Scale bar, 10 μm.

NET volume in LPS^{lo} mice 24 h after LPS (Fig. 5a,b). Most features of type 2 allergic airway inflammation, such as airway eosinophilia (Fig. 5c), HDM-specific type 2 immunity (Fig. 5d), peribronchial inflammation (Fig. 5e,f) and increased mucus production (Fig. 5g,h) were significantly reduced in DNase-, NEi- or Cl-amidine-treated LPS^{lo}-HDM mice compared to vehicle LPS^{lo}-HDM mice, except for LN production of IL-4 and IL-13, which was similar in DNase- and NEi-treated LPS^{lo}-HDM mice, respectively, compared to vehicle LPS^{lo}-HDM mice (Fig. 5d), and mucus production in NEi-treated LPS^{lo}-HDM mice compared to vehicle LPS^{lo}-HDM mice (Fig. 5g,h). These observations indicate that lung neutrophils and NETs from LPS^{lo} mice were mediating the pro-allergic effects of low-dose LPS on HDM-induced allergic asthma.

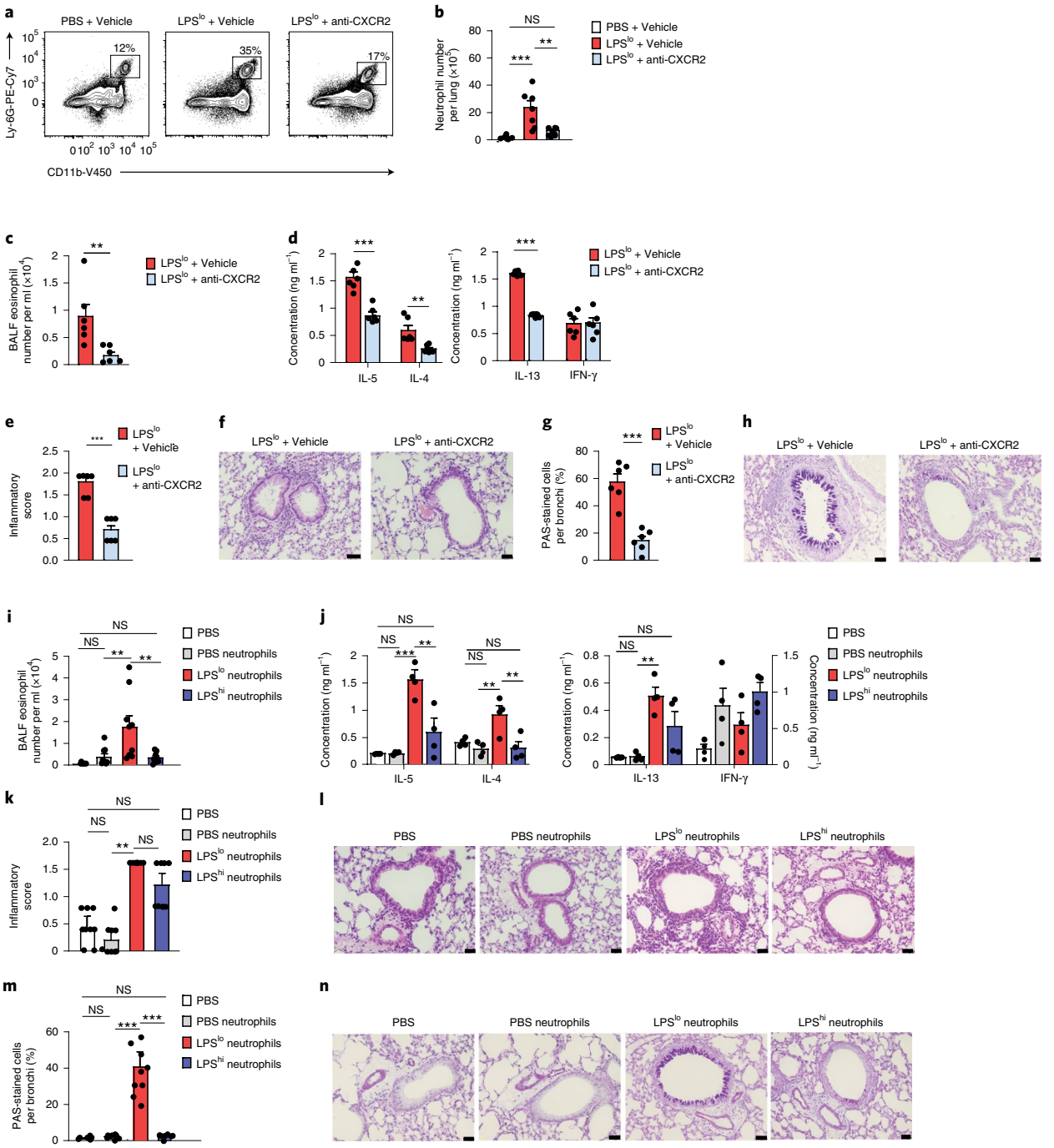


Fig. 4 | LPS^{lo} neutrophils mediate susceptibility to HDM-induced type 2 allergic airway inflammation. a, Representative dot plots of lung CD45^{+}CD11b^{hi}Ly-6G^{hi} neutrophils from vehicle or LPS^{lo} mice treated or not with Sch527123, a CXCR2 antagonist (anti-CXCR2), 2 h before and 4, 8 and 20 h after LPS, and analyzed 24 h after LPS^{lo}. Insets indicate percentage of cells within the gate. **b**, Absolute numbers of lung CD45^{+}CD11b^{hi}Ly-6G^{hi} neutrophils, as in **a**. **c**, Eosinophil cell counts in the BALF, assessed 3 d after the second HDM administration in LPS^{lo}-HDM mice treated or not with anti-CXCR2, 2 h before and 4 and 8 h after LPS^{lo}, and 2 h before and 4 h after i.n. sensitization with HDM. **d**, ELISA measurement of cytokine production by HDM-restimulated BLN cells of mice, as in **c**. **e**, Inflammatory score estimating perivascular and peribronchial inflammation, quantified from H&E-stained lung sections of mice, as in **c**. **f**, Representative H&E staining of lung sections of mice, as in **c**. **g**, Quantification of PAS-stained epithelial cells per bronchi showing airway mucus production in mice, as in **c**. **h**, Representative PAS staining of lung sections of mice, as in **c**. **i**, Eosinophil cell counts in BALF, assessed 3 d after the second HDM administration in mice transferred intratracheally with vehicle, LPS^{lo} and LPS^{hi} neutrophils and exposed to HDM. **j**, ELISA measurement of cytokine production by HDM-restimulated BLN cells of mice, as in **i**. **k**, Inflammatory score estimating perivascular and peribronchial inflammation, quantified from H&E-stained lung sections of mice, as in **i**. **l**, Representative H&E staining of lung sections of mice as in i. **m**, Quantification of PAS-stained epithelial cells per bronchi showing airway mucus production in mice, as in **i**. **n**, Representative PAS staining of lung sections of mice, as in **i**. (**b**–**e**,**g**,**i**–**k**,**m**, Data show mean + s.e.m. and are pooled from two independent experiments (**b**–**e**,**g**), each symbol representing individual mice ($n = 6$ per group) or ≥ 3 independent experiments (**i**–**k**,**m**), each symbol representing individual mice ($n = 9$ per group) (**i**,**k**,**m**) or independent experiments in which cells from 2–3 mice were pooled by group (**j**). *P* values were calculated with a one-way ANOVA with Tukey's *post hoc* test (**b**,**i**–**k**,**m**), a two-sided unpaired Student's *t*-test (**c**) or a two-sided Mann–Whitney test (**d**–**e**,**g**). $^{*}P < 0.05$; $^{**}P < 0.01$; $^{***}P < 0.001$. NS, not significant. Scale bar, 32 μm.

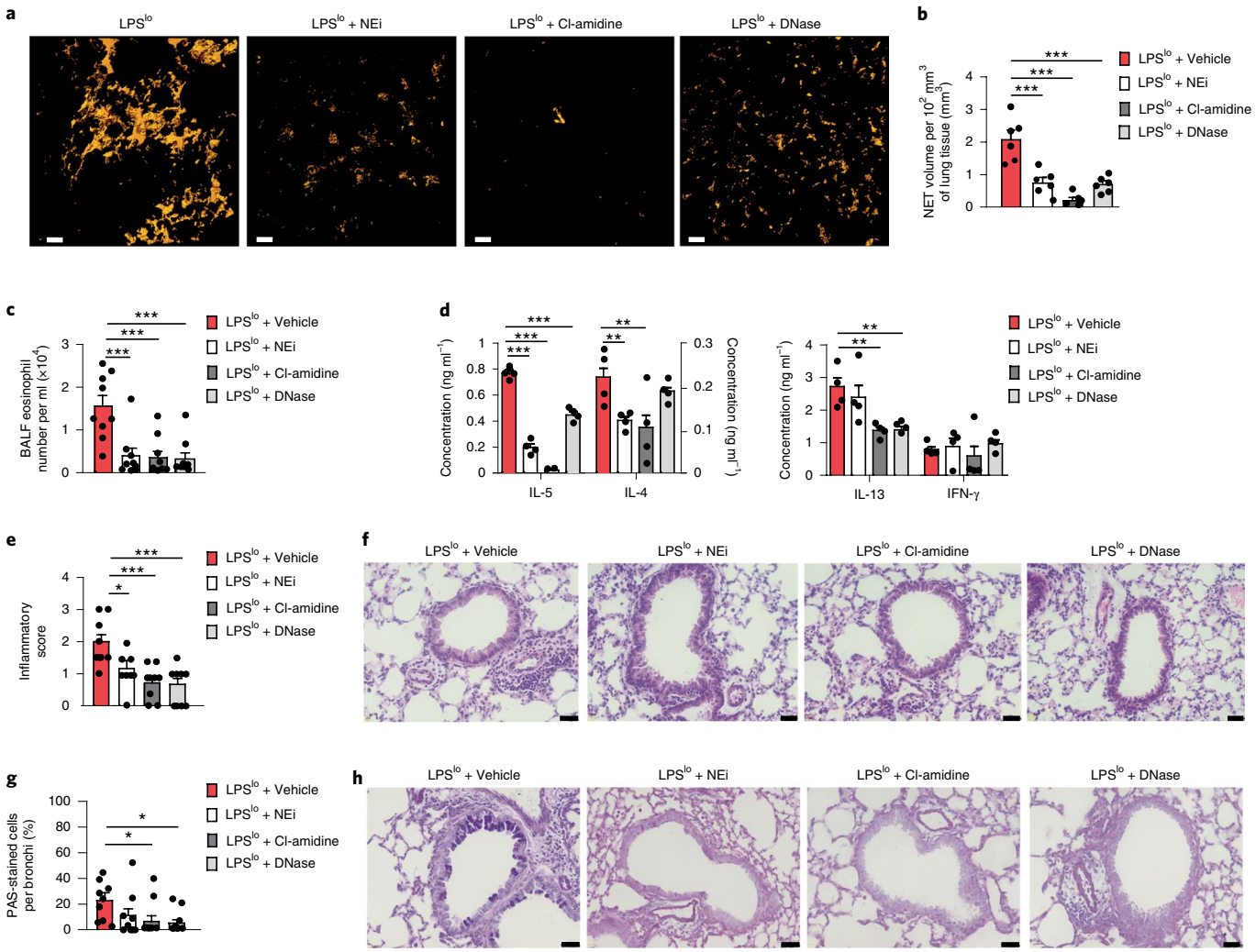


Fig. 5 | NETs mediate low-dose-LPS-triggered type 2 allergic airway inflammation to HDM. a, Three-dimensional modeling of Cit-H3$^+$MPO$^+$ NETs on lung sections, assessed 24 h after LPS^{lo} in mice treated i.p. with DNase 1 d before and at the time of LPS^{lo} treatment, or treated 4 times i.p. with NEi or Cl-amidine, every 12 h starting 1 d before LPS^{lo}. Pictures are representative of one of six lungs analyzed. **b**, Quantification of NET volume in lung sections of mice, as in **a**. **c**, Eosinophil cell counts in the BALF, assessed 3 d after the second HDM administration in LPS^{lo}-HDM mice treated i.p. with 4 daily injections of DNase, starting 1 d before LPS^{lo} treatment, or treated with 8 i.p. injections of NEi or Cl-amidine, every 12 hours starting 1 d before LPS^{lo} treatment. **d**, ELISA measurement of cytokine production by HDM-restimulated BLN cells of mice as in **c**. **e**, Inflammatory score estimating perivascular and peribronchial inflammation, quantified from H&E-stained lung sections of mice, as in **c**. **f**, Representative H&E staining of lung sections of mice, as in **c**. **g**, Quantification of PAS-stained epithelial cells per bronchi showing airway mucus production in mice, as in **c**. **h**, Representative PAS staining of lung sections of mice, as in **c**. **b**, Data show mean + s.e.m. as well as individual mice ($n = 6$ per group). **c**–**e**,**g**, Data show mean + s.e.m. and are pooled from 3–4 independent experiments, each symbol representing individual mice (**c**,**e**,**g**) ($n = 9$ per group) or independent experiments in which cells from 2–3 mice were pooled by group (**d**). *P* values were calculated with a one-way ANOVA with Tukey's post hoc test. $^*P < 0.05$; $^{**}P < 0.01$; $^{***}P < 0.001$. Scale bars, 10 µm (**a**); 32 µm (**f**,**h**).

NETs promote HDM uptake by CD11b$^+$Ly-6C$^+$ DCs. Given the predominant role played by lung DCs in the induction of T_H2 responses to HDM[31,32], we looked at their ability to take up HDM on exposure to vehicle, LPS^{lo} or LPS^{hi}. Twenty-four hours after LPS, we administered 40 µg of fluorescent-labeled AF647-HDM i.n., and the numbers of lung CD45$^+$CD11c^{hi}MHC-II^{hi}HDM$^+$ DCs were quantified 24 h later by flow cytometry. Lungs of LPS^{lo} mice exposed to AF647-HDM had greater numbers of CD11b$^+$Ly-6C$^+$ DCs, and to a lesser extent CD11b$^+$Ly-6C$^-$ DCs, that were AF647-HDM$^+$ than the lungs of vehicle or LPS^{hi} mice (Fig. 6a–c). Of note, the numbers of CD11b$^+$Ly-6C$^+$AF647-HDM$^+$ DCs were significantly reduced in DNase-, NEi- or Cl-amidine-treated LPS^{lo}-AF647-HDM mice as compared to vehicle LPS^{lo}-AF647-HDM mice (Fig. 6d), suggesting that NETs promoted HDM uptake by CD11b$^+$Ly-6C$^+$ DCs directly or indirectly.

To assess whether LPS^{lo} neutrophils modulated AF647-HDM uptake by CD11b$^+$Ly-6C$^+$ DCs directly, we co-cultured vehicle, LPS^{lo} or LPS^{hi} neutrophils with bone marrow–derived DCs (BMDCs), which contained both CD11b$^+$Ly-6C$^+$ and CD11b$^+$Ly-6C$^-$ BMDCs (Fig. 6e) and are known to induce type 2 sensitization to HDM when pulsed with HDM and reinjected into recipient animals[33]. Co-culture of AF647-HDM-treated BMDCs with LPS^{lo} neutrophils increased the uptake of AF647-HDM by CD11b$^+$Ly-6C$^+$ BMDCs, and to a lesser extent by CD11b$^+$Ly-6C$^-$ BMDCs, as compared to AF647-HDM-treated BMDCs alone (Fig. 6f). Co-culture of AF647-HDM-treated BMDCs with vehicle or LPS^{hi} neutrophils promoted a marginal increase in AF647-HDM uptake by CD11b$^+$Ly-6C$^+$ BMDCs compared to AF647-HDM-treated CD11b$^+$Ly-6C$^+$ BMDCs alone, which was significantly lower than that elicited by the co-culture

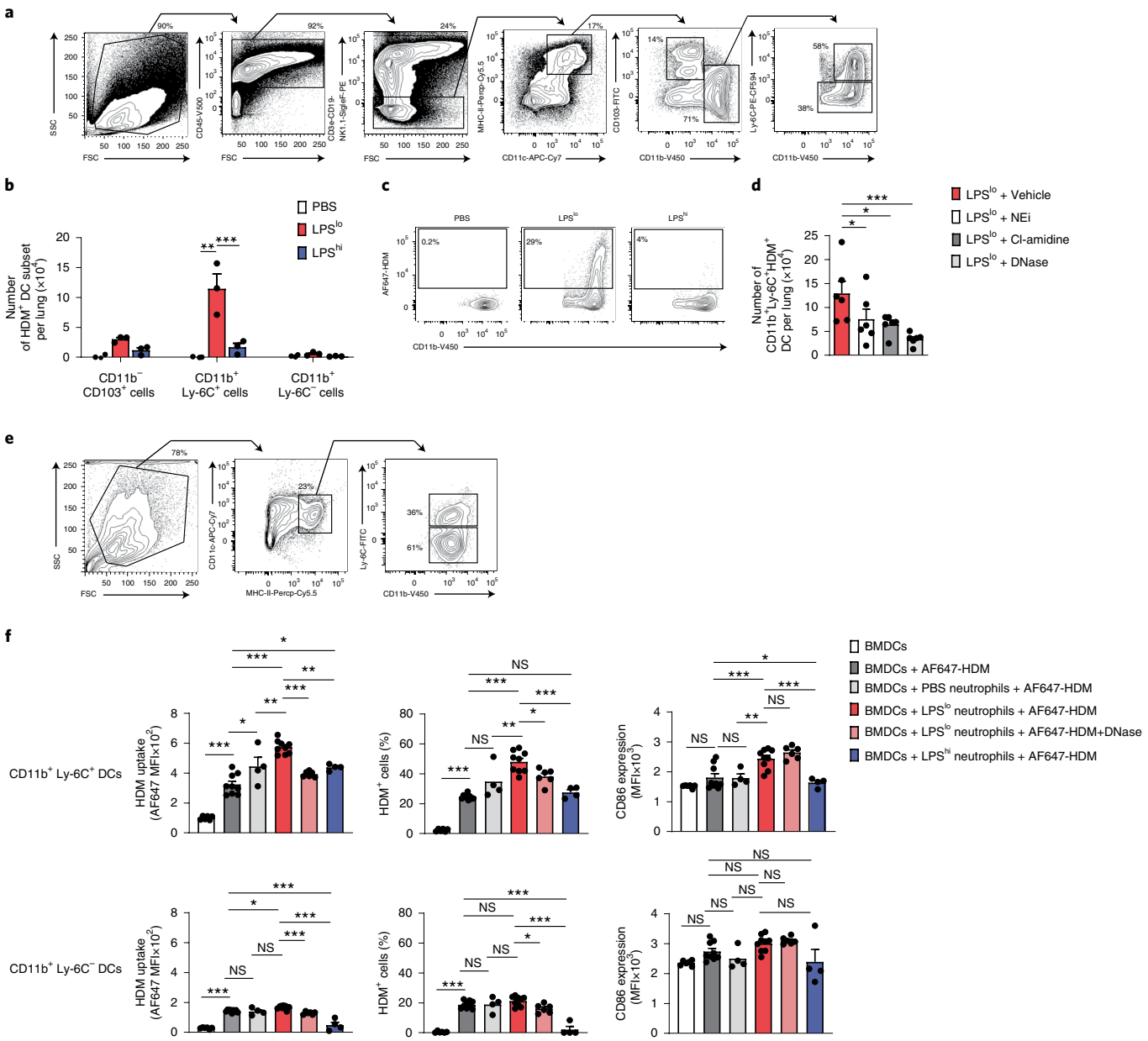


Fig. 6 | NETs released by LPS^{lo} neutrophils directly promote HDM uptake by CD11b$^+$Ly-6C$^+$ DCs. a, Representative gating strategy delineating lung DC subsets in vehicle-AF647-HDM, LPS^{lo}-AF647-HDM and LPS^{hi}-AF647-HDM mice, assessed 24 h after i.n. AF647-HDM. Lung cells from a LPS^{lo}-AF647-HDM mouse is shown. DCs were defined as CD45$^+$CD3e$^-$CD19$^-$NK1.1$^-$SiglecF$^-$MHC-II$^+$CD11c$^+$ cells and further divided into CD11b$^-$CD103$^+$, CD11b$^+$Ly-6C$^-$ and CD11b$^+$Ly-6C$^+$ DCs. **b**, Absolute numbers of lung AF647-HDM$^+$ DC subsets in mice, as in **a**. **c**, Representative dot plots showing AF647-HDM MFI in lung CD11b$^+$Ly-6C$^+$ DCs from mice, as in **a**. **d**, Absolute numbers of lung CD11b$^+$Ly-6C$^+$AF647-HDM$^+$ DCs, assessed 24 h after i.n. AF647-HDM in LPS^{lo}-AF647-HDM mice treated i.p. with 3 daily injections of DNase, starting 1 d before LPS^{lo} treatment, or treated with 5 i.p. injections of NEi or Cl-amidine, every 12 h starting 1 d before LPS^{lo} treatment. **e**, Representative gating strategy delineating BMDC subsets. BMDCs were defined as MHC$^-$II$^+$CD11c$^+$ cells and further divided into CD11b$^+$Ly-6C$^-$ and CD11b$^+$Ly-6C$^+$ subsets. **f**, MFI of AF647-HDM (left), percentage of AF647-HDM$^+$ cells (middle), and CD86 expression (right) in CD11b$^+$Ly-6C$^+$ (top) and CD11b$^+$Ly-6C$^-$ (bottom) BMDCs, assessed 12 h after treatment with AF647-HDM and after co-culture with vehicle, LPS^{hi} or LPS^{lo} neutrophils in the presence or absence of DNase. **b**,**d**,**f**, Data show mean + s.e.m. and are pooled from ≥ 3 independent experiments, each symbol representing independent experiments in which cells from 3–5 mice were pooled by group (**b**,**d**) (b,d: $n = 3,6$, respectively) or independent co-culture experiments (**f**) (BMDCs; BMDCs + AF647-HDM; BMDCs + PBS neutrophils + AF647-HDM; BMDCs + LPS^{lo} neutrophils + AF647-HDM; BMDCs + LPS^{lo} neutrophils + AF647-HDM + DNase; BMDCs + LPS^{hi} neutrophils + AF647-HDM: $n = 6;9;4;9;6;4$, respectively). *P* values were calculated with a two-way (**b**) or a one-way ANOVA with Tukey's post hoc test (**d**,**f**). $^*P < 0.05$; $^{**}P < 0.01$; $^{***}P < 0.001$. NS, not significant.

of AF647-HDM-treated BMDCs with LPS^{lo} neutrophils (Fig. 6f). AF647-HDM uptake, especially by CD11b$^+$Ly-6C$^+$ BMDCs, was significantly diminished when DNase was added to the co-culture of BMDCs with LPS^{lo} neutrophils (Fig. 6f), indicating that the process was dependent on NETs. Co-culture of BMDCs with LPS^{lo} neutrophils, but not with vehicle or LPS^{hi} neutrophils, promoted the expression of the pro-T_H2 co-stimulatory molecule CD86 (refs. [34,35]) on CD11b$^+$Ly-6C$^+$ BMDCs, and this effect was not affected by DNase treatment (Fig. 6f). Thus, LPS^{lo} neutrophils acted on CD11b$^+$Ly-6C$^+$ DCs directly to promote AF647-HDM uptake through NET-dependent mechanisms.

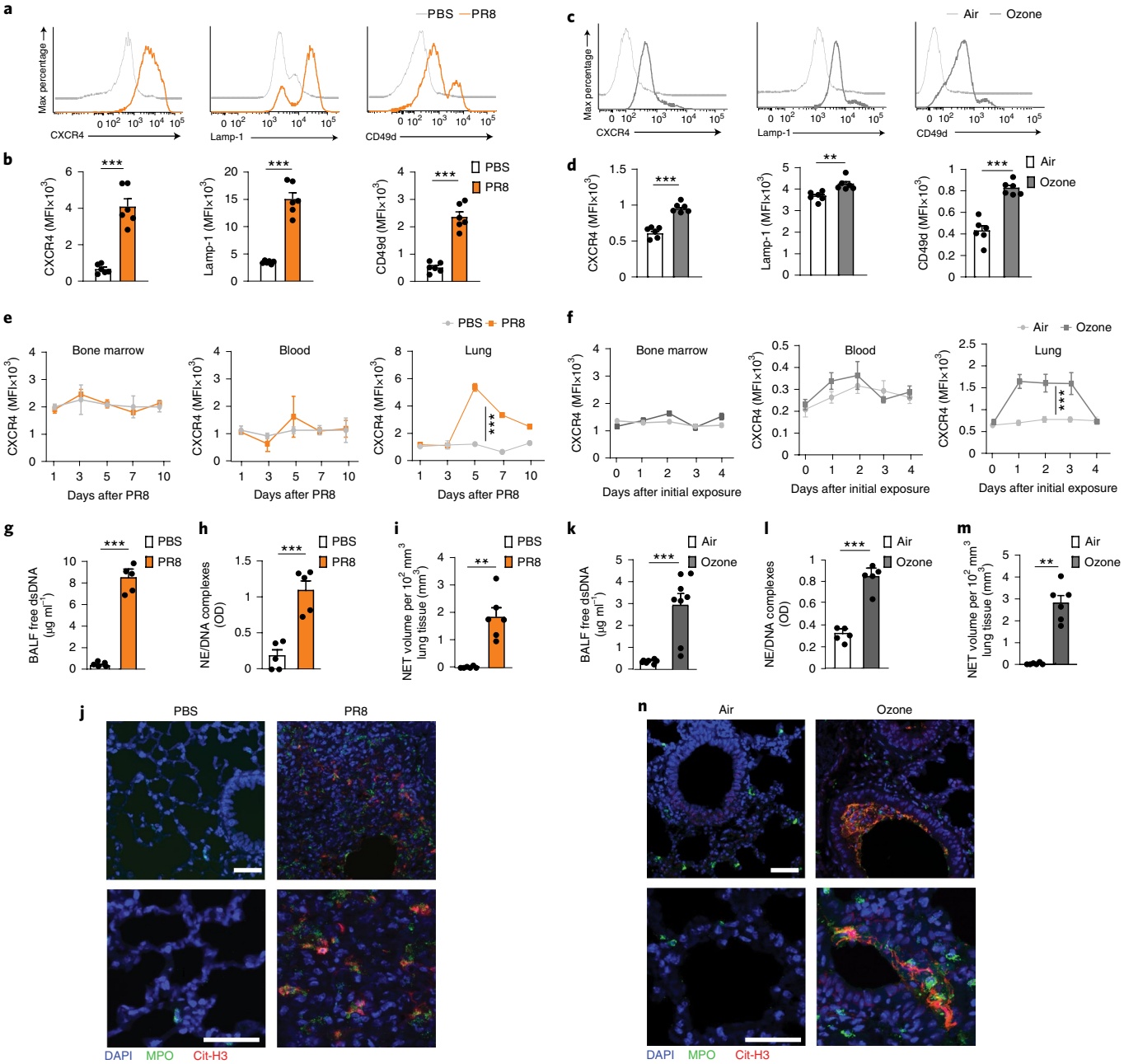


Fig. 7 | Influenza virus infection and ozone exposure instruct recruited lung CXCR4^{hi} neutrophils to release NETs. a,**c**, Representative histograms of CXCR4, Lamp-1 and CD49d expression by lung CD45^{+}CD11b^{hi}Ly-6G^{hi} neutrophils 7 d after influenza virus (PR8) infection (**a**) or 24 h after 3 daily ozone exposures (**c**). **b**,**d**, MFI showing quantification of CXCR4, CD49d and Lamp-1 expression by lung CD45^{+}CD11b^{hi}Ly-6G^{hi} neutrophils as in **a** and **c**, respectively. **e**,**f**, Kinetic analysis of CXCR4 expression by bone marrow, blood and lung CD45^{+}CD11b^{hi}Ly-6G^{hi} neutrophils after PR8 infection (**e**) or ozone exposure (**f**), as in **a**. **g**,**k**, Levels of extracellular dsDNA in the BALF of PBS-injected and PR8-infected mice (**g**), 7 d after PR8, or air- and ozone-exposed mice, 24 h after 3 daily ozone exposures (**k**). **h**,**l**, ELISA measurement of NE–DNA complexes in the BALF of mice, as in **g** and **k**, respectively. **i**,**m**, Confocal microscopy stainings of Cit-H3^{+}MPO^{+} NETs on lung sections of mice, as in **g** and **k**, respectively. Pictures are representative of one of >5 lungs analyzed. **j**,**n**, Quantification of NET volume in lung sections of mice, as in **g** and **k**, respectively. (**b**,**d**–**i**,**k**–**m**) Data show mean + s.e.m. and are pooled from 2–3 independent experiments (**b**,**d**,**g**–**i**,**k**–**m**) (b,d,g,h,i,k,l,m: $n = 6,6,5,5,6,8,5,6$) mice per group, respectively) or 2 independent experiments per time point analyzed (**e**,**f**) ($n = 4$ mice per time point). *P* values were calculated using an unpaired two-tailed Student's *t*-test (**b**,**d**,**g**–**i**,**k**–**m**) or a one-way ANOVA that compares PR8-infected or ozone-exposed versus control counterparts (**e**,**f**). $^{**}P < 0.01$; $^{***}P < 0.001$. NS, not significant; OD, optical density. Scale bars, 50 μm.

Other pro-allergic factors promote allergic asthma via NETs. Next, we tested whether NET-prone CXCR4^{hi} neutrophils were associated with additional pro-allergic conditions. Besides low exposure to microbial products, respiratory viral infections[6] and air pollution[7] also represent risk factors for allergic asthma in humans. In mice, acute respiratory infection with influenza virus[36] or exposure to ozone[37] promote allergic airway inflammation to HDM or ovalbumin, respectively. BALB/c mice infected i.n. with 5 plaque-forming units (PFU) of influenza A virus H1N1 strain PR8/34 (PR8) had decreased body weight at day 7 (Supplementary Fig. 7a,b) and

increased lung viral RNA expression (Supplementary Fig. 7c) and numbers of CD45$^+$CD11b^{hi}Ly-6G^{hi} neutrophils (Supplementary Fig. 7d) between 3 and 7 d after infection. Similarly, BALB/c mice exposed for 3 d to 2 ppm ozone during 3 h also had increased lung neutrophil numbers 24 h after the last exposure (Supplementary Fig. 7e,f). Seven days after PR8 or 24 h after ozone exposure, these neutrophils had increased expression of CXCR4, Lamp-1 and CD49d as compared to neutrophils from uninfected or air-exposed control mice (Fig. 7a–d), suggesting shared phenotypical similarities with LPS^{lo} neutrophils. In addition, CXCR4^{hi} neutrophils were only found in the lung and could not be detected in the blood or BM (Fig. 7e,f), suggesting local imprinting. NETs were also found in the lungs of mice infected with PR8 or exposed to ozone (Fig. 7g–n and Supplementary Fig. 7g–k), suggesting that exposure to other pro-allergic factors triggered the accumulation of NET-prone CXCR4^{hi} neutrophils in the lungs.

Next, we instilled PR8-infected mice i.n. with 40 µg of HDM 7 d after PR8 and with 10 µg of HDM 7 d later (PR8-HDM). To test the contribution of NETs to PR8-triggered allergic asthma, PR8-HDM mice were treated daily for 12 d with DNase i.p., starting 5 d after PR8. Alternatively, PR8-HDM mice were treated every 12 h with NEi or Cl-amidine i.p. for the same duration as for DNase. Three days after the HDM challenge, we observed increased susceptibility of PR8-HDM mice to develop airway eosinophilia and HDM-specific IgG1 (Fig. 8a), HDM-specific type 2 immunity (Fig. 8b) and goblet cell hyperplasia (Fig. 8c,d), while administration of HDM without pre-exposure to PR8 did not induce features of allergic asthma and treatments of PR8-HDM mice with DNase, NEi and Cl-amidine resulted in a significant decrease of nearly all features of allergic asthma compared to vehicle PR8-HDM mice, except for LN production of IL-13, which was similar in DNase-treated and vehicle PR8-HDM mice (Fig. 8b). In addition, while we observed higher numbers of lung CD11b$^+$Ly-6C$^+$AF647-HDM$^+$ DCs in PR8-AF647-HDM mice than in uninfected AF647-HDM-treated controls 24 h after AF647-HDM, these numbers were significantly decreased in DNase-, NEi- and Cl-amidine-treated PR8-AF647-HDM mice compared to vehicle PR8-AF647-HDM controls (Fig. 8e).

We also instilled ozone-exposed mice i.n. with 40 µg of HDM 1 d after the last ozone treatment and with 10 µg of HDM 7 d later (ozone-HDM). Some ozone-HDM mice were also treated daily for 4 d with DNase i.p., starting the first day of ozone exposure. Alternatively, ozone-HDM mice were treated every 12 h with NEi or Cl-amidine i.p. for the same duration as for DNase. Three days after the HDM challenge, we observed increased susceptibility of ozone-HDM mice to develop airway eosinophilia and HDM-specific IgG1 (Fig. 8f), HDM-specific type 2 immunity (Fig. 8g), goblet cell hyperplasia (Fig. 8h,i) and peribronchial inflammation (Supplementary Fig. 8), while administration of HDM without pre-exposure to ozone did not induce features of allergic asthma and treatments of ozone-HDM mice with DNase, NEi and Cl-amidine resulted in a significant decrease of all the features of allergic asthma tested (Fig. 8f–i and Supplementary Fig. 8). In addition, while we observed higher numbers of lung CD11b$^+$Ly-6C$^+$AF647-HDM$^+$ DCs in ozone-AF647-HDM mice than in air-exposed AF647-HDM-treated controls 24 h after AF647-HDM, these numbers were significantly decreased in DNase-, NEi- and Cl-amidine-treated ozone-AF647-HDM mice compared to vehicle ozone-AF647-HDM controls (Fig. 8j).

These observations suggested that NETs promoted AF647-HDM uptake by lung CD11b$^+$Ly-6C$^+$ DCs and mediated allergic airway inflammation triggered by flu infection or ozone exposure.

Discussion

Here we showed that neutrophils have an important role in type 2 allergic immunity and link pro-allergic environmental conditions and host allergic susceptibility. We showed that airway exposure to low-dose LPS, influenza virus infection and ozone exposure in mice induced the accumulation of NET-releasing CXCR4^{hi} neutrophils in the lung. These neutrophils promoted the uptake of HDM by lung CD11b$^+$Ly-6C$^+$ DCs and increased susceptibility to allergic asthma.

LPS measurements have been used in epidemiological studies related to the 'hygiene hypothesis', suggesting that an LPS-rich environment is associated with reduced risk of atopy and asthma, while LPS-poor environments represent a risk factor for the development of asthma[8,38]. The 'hygienic' model used here is an adaptation of a previous model[21], in which priming with a low or high dose of LPS biased the immune response to ovalbumin towards a T_H2 or T_H1 profile, respectively. Here, we found that exposure to a low dose of LPS in BALB/c mice potentiated HDM-induced type 2 allergic asthma, while priming with a higher dose of LPS[22] had no substantial effect.

Airway exposure to low-dose LPS in mice triggered NET-releasing CXCR4^{hi} neutrophils in the lung. These neutrophils shared similarities with 'aged' neutrophils, a subset of NET-prone CXCR4^{hi} neutrophils found in the blood[25,26]. Kinetic analyses of CXCR4 expression on lung, blood and BM neutrophils indicated that neutrophils were recruited to the lung and instructed locally. This indicates that CXCR4^{hi} neutrophils, rather than representing a subset, are in a transient state of activation that depends on a local stimulus (that is, low-dose LPS). Our data argue in favor of the notion that neutrophils are heterogeneous, plastic and adaptable to context-specific cues to exert particular functions[14]. We found that these locally instructed CXCR4^{hi} neutrophils represented early and critical players in the initiation of type 2 allergic asthma against HDM allergens. Given the central role of epithelial-derived alarmins, including IL-33, IL-25 and TSLP in the initiation of type 2 allergic immunity[39], it would be interesting to test their respective contributions to the imprinting of CXCR4^{hi} neutrophils.

We used DNase, NEi and Cl-amidine to assess the functional importance of NETs in the initiation of allergic asthma. None of these approaches are fully specific for NETs[36]. Cl-amidine inhibits the activity of PAD4, which is implicated in chromatin reorganization and is expressed in many cell types. Treatment with Cl-amidine may lead to decreased activity of citrullinated histone proteins rather than NET impairment[19]. In addition, the biological activity of the inhibitors may not be optimal in the tissue and could be influenced by factors that are inherent to the experimental models used. However, treatment with DNase, NEi and Cl-amidine impaired NETs and had the same global outcome on the development of HDM-induced asthma, suggesting that NETs could be mediating the onset of allergic airway inflammation to HDM in the models tested here.

Low-dose LPS, influenza virus infection and ozone exposure were associated with an increased uptake of fluorescent-labeled HDM by CD11b$^+$Ly-6C$^+$ DCs, an important step in the initiation of HDM-specific type 2 responses[31,32]. Allergen uptake was significantly reduced in NET-targeted mice, supporting the idea that NETs can directly or indirectly modulate this process. Ex vivo co-culture experiments with lung neutrophils and BMDCs further indicated that NETs derived from LPS^{lo} neutrophils could directly promote HDM uptake by CD11b$^+$Ly-6C$^+$ DCs. Our study is in accordance with reports that extracellular host DNA, the main NET component, is a potent signal that promotes the activation of DCs and type 2 immune responses[20,40].

Whether CXCR4^{hi} neutrophils and NETs can trigger type 2 sensitization against other type 2-inducing stimuli, such as fungal proteases, food allergens, helminths or additional pro-allergic factors (such as other respiratory viruses, exhaust particles, cigarette smoke) in BALB/c or other genetic backgrounds remains unclear[17]. In humans, neutrophils are important immune-modulating cells in the effector phase of severe asthma, which is characterized by neutrophilic inflammation, high expression of IL-17 and resistance to corticosteroids[16–19]. Whether particular NET-releasing neutrophils contribute to the initiation of type 2 allergic asthma in humans remains unknown. A prospective Danish study found that the

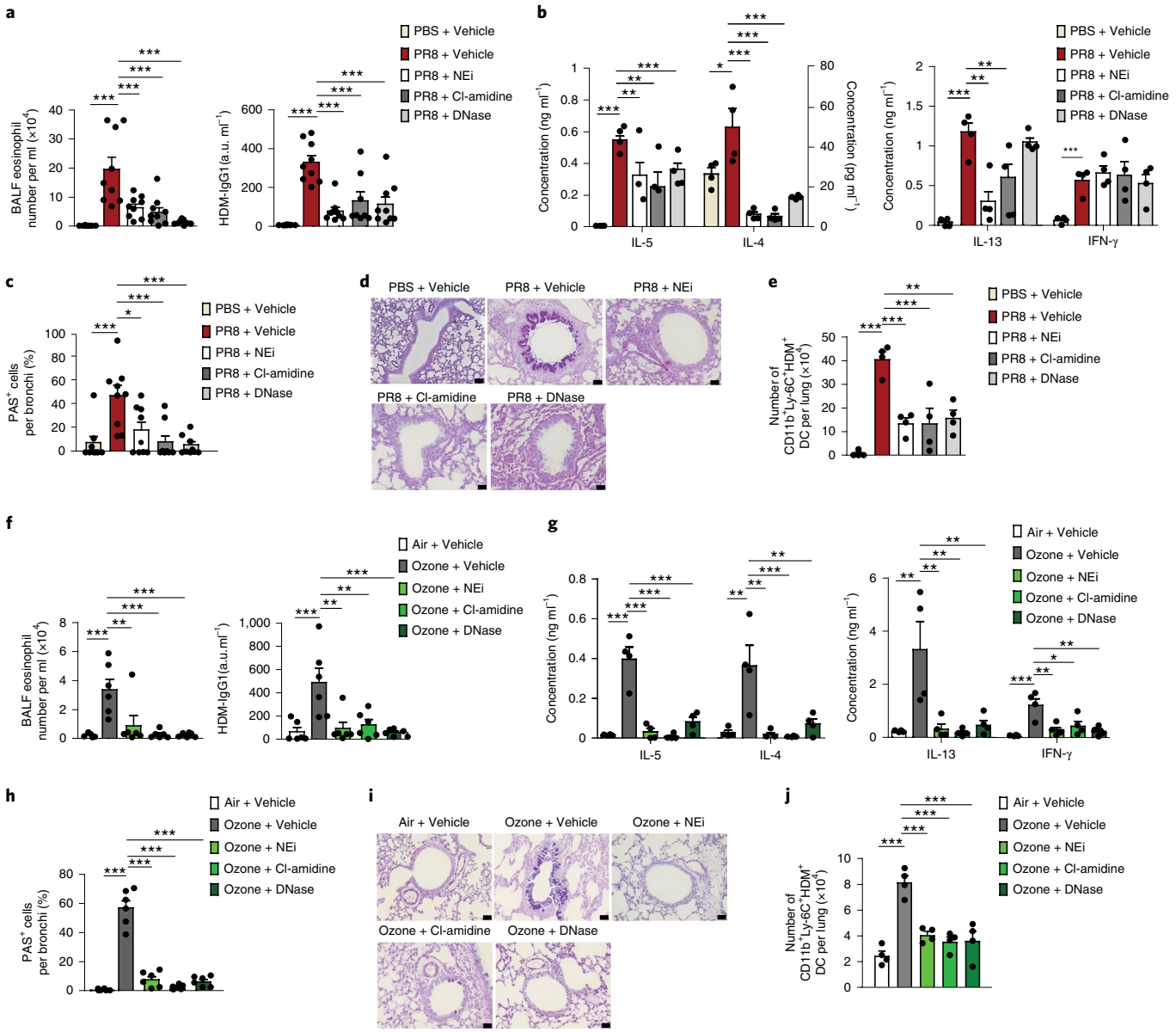


Fig. 8 | NETs mediate influenza virus- and ozone-potentiated type 2 allergic airway inflammation to HDM. a, Eosinophil cell counts in the BALF (left) and ELISA measurement of HDM-specific IgG1 in the serum (right), assessed 3 d after the second HDM administration in vehicle-HDM and PR8-HDM mice treated daily for 12 d with DNase i.p., starting 5 d after PR8, or treated every 12 h with NEi or Cl-amidine i.p., for the same duration as for DNase. **b**, ELISA measurement of cytokine production by HDM-restimulated BLN cells of mice, as in **a**. **c**, Quantification of PAS-stained epithelial cells per bronchi showing airway mucus production in mice, as in **a**. **d**, Representative PAS staining of lung sections of mice, as in **a**. **e**, Absolute numbers of lung CD11b⁺Ly-6C⁺AF647-HDM⁺ DCs assessed 8 d after PR8 and 24 h after AF647-HDM in vehicle-AF647-HDM and PR8-AF647-HDM mice treated daily for 3 d with DNase i.p., starting 5 d after PR8, or treated every 12 h with NEi or Cl-amidine i.p., for the same duration as for DNase. **f**, Eosinophil cell counts in the BALF (left) and ELISA measurement of HDM-specific IgG1 in the serum (right), assessed 3 d after the second HDM administration in vehicle-HDM and ozone-HDM mice treated daily for 4 d with DNase i.p., starting the first day of ozone exposure, or treated every 12 h with NEi or Cl-amidine i.p., for the same duration as for DNase. **g**, ELISA measurement of cytokine production by HDM-restimulated BLN cells of mice as in **f**. **h**, Quantification of PAS-stained epithelial cells per bronchi showing airway mucus production in mice, as in **f**. **i**, Representative PAS staining of lung sections of mice, as in **f**. **j**, Absolute numbers of lung CD11b⁺Ly-6C⁺AF647-HDM⁺ DCs assessed 2 d after the last ozone exposure and 24 h after AF647-HDM in mice, as in **f**. **a**–**c**,**e**,**f**–**h**,**j** Data show mean + s.e.m. and are pooled from 2-3 independent experiments, each symbol representing individual mice (**a**,**c**,**f**,**h**) (a,b,e,g,h,k: $n = 9,9,6,6$ mice per group, respectively) or independent experiments in which cells from 2–4 mice were pooled by group (**b**,**e**,**g**,**j**). *P* values were calculated with a one-way ANOVA with Tukey's post hoc test. $^*P < 0.05$; $^{**}P < 0.01$; $^{***}P < 0.001$. a.u., arbitrary unit. Scale bar, 32 μm.

number of respiratory infections in early life, but not the particular viral trigger, was associated with asthma development[41]. The authors postulated that a host-derived factor might underlie the increased allergic susceptibility[41]. Our results suggest that the accumulation of NET-prone neutrophils could be such a host-associated factor. In addition, blood neutrophils from Hutterite children, who are raised in an environment poor in LPS and are prone to develop allergies, have higher expression of CXCR4 than blood neutrophils from Amish children, who live in LPS-rich homes and are protected from allergies[38]. While lung neutrophils have not been assessed in these

children, it is tempting to speculate that environmental risk factors may promote allergic airway sensitization in humans by inducing NET-prone CXCR4^{hi} neutrophils, which increase host susceptibility to mount type 2 allergic responses towards aeroallergens.

Online content

Any methods, additional references, Nature Research reporting summaries, source data, statements of code and data availability and associated accession codes are available at https://doi.org/10.1038/s41590-019-0496-9.

Received: 4 June 2018; Accepted: 15 August 2019;
Published online: 07 October 2019

References

1. Braman, S. S. The global burden of asthma. *Chest* **130**, 4s–12s (2006).
2. Galli, S. J., Tsai, M. & Piliponsky, A. M. The development of allergic inflammation. *Nature* **454**, 445–454 (2008).
3. Vercelli, D. Discovering susceptibility genes for asthma and allergy. *Nat. Rev. Immunol.* **8**, 169–182 (2008).
4. Eder, W., Ege, M. J. & von Mutius, E. The asthma epidemic. *N. Engl. J. Med.* **355**, 2226–2235 (2006).
5. Platts-Mills, T. A. The allergy epidemics: 1870–2010. *J. Allergy Clin. Immunol.* **136**, 3–13 (2015).
6. Busse, W. W., Lemanske, R. F. Jr. & Gern, J. E. Role of viral respiratory infections in asthma and asthma exacerbations. *Lancet* **376**, 826–834 (2010).
7. Peden, D. B. The epidemiology and genetics of asthma risk associated with air pollution. *J. Allergy Clin. Immunol.* **115**, 213–219 (2005). quiz 220.
8. Braun-Fahrlander, C. et al. Environmental exposure to endotoxin and its relation to asthma in school-age children. *N. Engl. J. Med.* **347**, 869–877 (2002).
9. Strachan, D. P. Family size, infection and atopy: the first decade of the 'hygiene hypothesis'. *Thorax* **55**, S2–S10 (2000).
10. Lloyd, C. M. & Snelgrove, R. J. Type 2 immunity: expanding our view. *Sci. Immunol.* **3**, eaat1604 (2018).
11. Lambrecht, B. N. & Hammad, H. The immunology of asthma. *Nat. Immunol.* **16**, 45–56 (2015).
12. Gregory, L. G. & Lloyd, C. M. Orchestrating house dust mite-associated allergy in the lung. *Trends Immunol.* **32**, 402–411 (2011).
13. Locksley, R. M. Asthma and allergic inflammation. *Cell* **140**, 777–783 (2010).
14. Ng, L. G., Ostuni, R. & Hidalgo, A. Heterogeneity of neutrophils. *Nat. Rev. Immunol.* **19**, 255–265 (2019).
15. Papayannopoulos, V. Neutrophil extracellular traps in immunity and disease. *Nat. Rev. Immunol.* **18**, 134–147 (2018).
16. Krishnamoorthy, N. et al. Neutrophil cytoplasts induce TH17 differentiation and skew inflammation toward neutrophilia in severe asthma. *Sci. Immunol.* **3**, eaao4747 (2018).
17. Radermecker, C., Louis, R., Bureau, F. & Marichal, T. Role of neutrophils in allergic asthma. *Curr. Opin. Immunol.* **54**, 28–34 (2018).
18. Wang, Y. H. & Wills-Karp, M. The potential role of interleukin-17 in severe asthma. *Curr. Allergy Asthma Rep.* **11**, 388–394 (2011).
19. Lachowicz-Scroggins, M. E. et al. Extracellular DNA, neutrophil extracellular traps, and inflammasome activation in severe asthma. *Am. J. Respir. Crit. Care Med.* **199**, 1076–1085 (2019).
20. Toussaint, M. et al. Host DNA released by NETosis promotes rhinovirus-induced type-2 allergic asthma exacerbation. *Nat. Med.* **23**, 681–691 (2017).
21. Eisenbarth, S. C. et al. Lipopolysaccharide-enhanced, toll-like receptor 4-dependent T helper cell type 2 responses to inhaled antigen. *J. Exp. Med.* **196**, 1645–1651 (2002).
22. Schuijs, M. J. et al. Farm dust and endotoxin protect against allergy through A20 induction in lung epithelial cells. *Science* **349**, 1106–1110 (2015).
23. Zheng, G. X. et al. Massively parallel digital transcriptional profiling of single cells. *Nat. Commun.* **8**, 14049 (2017).
24. Remijsen, Q. et al. Neutrophil extracellular trap cell death requires both autophagy and superoxide generation. *Cell Res.* **21**, 290–304 (2011).
25. Adrover, J. M., Nicolas-Avila, J. A. & Hidalgo, A. Aging: a temporal dimension for neutrophils. *Trends Immunol.* **37**, 334–345 (2016).
26. Casanova-Acebes, M. et al. Rhythmic modulation of the hematopoietic niche through neutrophil clearance. *Cell* **153**, 1025–1035 (2013).
27. Dwyer, M. P. et al. Discovery of 2-hydroxy-N,N-dimethyl-3-{2-[[(R)-1-(5- methylfuran-2-yl)propyl]amino]-3,4-dioxocyclobut-1-enylamino} benzamide (SCH527123): a potent, orally bioavailable CXCR2/CXCR1 receptor antagonist. *J. Med. Chem.* **49**, 7603–7606 (2006).
28. Reutershan, J. et al. Critical role of endothelial CXCR2 in LPS-induced neutrophil migration into the lung. *J. Clin. Invest.* **116**, 695–702 (2006).
29. Cools-Lartigue, J. et al. Neutrophil extracellular traps sequester circulating tumor cells and promote metastasis. *J. Clin. Invest.* **123**, 3446–3458 (2013).
30. Wang, Y. et al. Histone hypercitrullination mediates chromatin decondensation and neutrophil extracellular trap formation. *J. Cell Biol.* **184**, 205–213 (2009).
31. Mesnil, C. et al. Resident CD11b^{+}Ly6C^{-} lung dendritic cells are responsible for allergic airway sensitization to house dust mite in mice. *PloS ONE* **7**, e53242 (2012).
32. Plantinga, M. et al. Conventional and monocyte-derived CD11b^{+} dendritic cells initiate and maintain T helper 2 cell-mediated immunity to house dust mite allergen. *Immunity* **38**, 322–335 (2013).
33. Marichal, T. et al. Interferon response factor 3 is essential for house dust mite-induced airway allergy. *J. Allergy Clin. Immunol.* **126**, 836–844.e13 (2010).
34. Larché, M. et al. Costimulation through CD86 is involved in airway antigen-presenting cell and T cell responses to allergen in atopic asthmatics. *J. Immunol.* **161**, 6375–6382 (1998).
35. Janss, T. et al. Interferon response factor-3 promotes the pro-Th2 activity of mouse lung CD11b^{+} conventional dendritic cells in response to house dust mite allergens. *Eur. J. Immunol.* **46**, 2614–2628 (2016).
36. Al-Garawi, A. A. et al. Acute, but not resolved, influenza A infection enhances susceptibility to house dust mite-induced allergic disease. *J. Immunol.* **182**, 3095–3104 (2009).
37. Hollingsworth, J. W. et al. Ozone activates pulmonary dendritic cells and promotes allergic sensitization through a Toll-like receptor 4-dependent mechanism. *J. Allergy Clin. Immunol.* **125**, 1167–1170 (2010).
38. Stein, M. M. et al. Innate immunity and asthma risk in amish and hutterite farm children. *N. Engl. J. Med.* **375**, 411–421 (2016).
39. Roan, F., Obata-Ninomiya, K. & Ziegler, S. F. Epithelial cell-derived cytokines: more than just signaling the alarm. *J. Clin. Invest.* **129**, 1441–1451 (2019).
40. Marichal, T. et al. DNA released from dying host cells mediates aluminum adjuvant activity. *Nat. Med.* **17**, 996–1002 (2011).
41. Bonnelykke, K., Vissing, N. H., Sevelsted, A., Johnston, S. L. & Bisgaard, H. Association between respiratory infections in early life and later asthma is independent of virus type. *J. Allergy Clin. Immunol.* **136**, 81–86.e4 (2015).

Acknowledgments

We thank F. Trottein (Pasteur Institute, Lille, France) for providing us with the Influenza A virus H1N1 PR8/34 strain; S. Ormenese, R. Stefan, J.-J. Goval and A. Hego from the GIGA Flow Cytometry and Cell Imaging Platform; P. Drion and all staff members from the GIGA Mouse facility and Transgenics Platform; C. Humblet and staff members from the GIGA Immunohistology Platform; B. Charloteaux, M. Deckers, L. Karim and members from the GIGA Genomics Platform; C. Desmet and D. Pirottin for insightful discussions; and C. François, R. Fares and I. Sbai for their excellent technical and administrative support. C.Radermecker and C.S. were research fellows of the F.R.S-FNRS; S.L.J. was supported by a Chair from Asthma UK (no. CH11SJ, to S.L.J.) and Medical Research Council Center grant (no. G1000758, to S.L.J.); F.B. is supported by the F.R.S.-FNRS for the FRFS-WELBIO (grant no. CR-2012S-01R to F.B.) and by an Excellence Of Science (EOS) grant. T.M. is a Research Associate of the F.R.S.-FNRS and is supported by an 'Incentive Grant for Scientific Research' of the F.R.S.-FNRS (grant no. F.4508.18 to T.M.), by the FRFS-WELBIO (grant no. CR-2017s-04 to T.M.), by the Acteria Foundation and by an ERC Starting Grant (grant no. ERC-StG-2018 IM-ID 801823 to T.M.).

Author contributions

C.Radermecker, T.M. and F.B. conceived the project. T.M., F.B., M.T., C.Radermecker and C.S. were involved in experimental design. C.Radermecker and C.S. realized most experiments, compiled the data and contributed equally to this work. P.M., C.Ruscitti and J.S. were involved in (bone marrow-derived) dendritic cell-related experiments. M.T. and S.L.J. were involved in experiments aiming at detecting and inhibiting NETs. C.V., F.P., N.R. and D.C. contributed to experiments involving ozone exposure and invasive measurements of airway function. T.M. analyzed scRNA-seq data with the help of the GIGA Genomics Platform. C.Radermecker and T.M. prepared the figures, and T.M. wrote the manuscript. All authors provided feedback on the manuscript.

Competing interests

The authors declare no competing interests.

Additional information

Supplementary information is available for this paper at https://doi.org/10.1038/s41590-019-0496-9.

Correspondence and requests for materials should be addressed to F.B. or T.M.

Peer review information Ioana Visan was the primary editor on this article and managed its editorial process and peer review in collaboration with the rest of the editorial team.

Reprints and permissions information is available at www.nature.com/reprints.

Publisher's note Springer Nature remains neutral with regard to jurisdictional claims in published maps and institutional affiliations.

© The Author(s), under exclusive licence to Springer Nature America, Inc. 2019

Methods

Mice. Female BALB/c mice were purchased from Janvier Laboratories. Age-matched, 6- to 10-week-old mice were used for experiments. Mice were housed under specific pathogen-free conditions and maintained in a 12-h light–dark cycle with food and water ad libitum. All animal experiments described in this study were reviewed and approved by the Institutional Animal Care and Use Committee of the University of Liège. The 'Guide for the Care and Use of Laboratory Animals', prepared by the Institute of Laboratory Animal Resources, National Research Council, and published by the National Academy Press, as well as European and local legislations, were followed carefully.

Reagents and antibodies. 2.4G2 Fc receptor-blocking antibodies were produced in house. Anti-mouse FITC- and V500-conjugated anti-CD45.2 (clone 104), PE-conjugated anti-CD3 (clone 142-2C11), PE-conjugated anti-CD19 (clone 1D3), PE-conjugated anti-NK1.1 (clone pk136), PE-conjugated anti-SiglecF (clone E50-2440), PE-conjugated anti-Ly-6G (clone RB6-8C5), eFluor450- and PE-Cy7-conjugated anti-CD11b (clone M1/70), PE-Cy7-conjugated anti-Ly-6G (clone 1A8), APC-Cy7-conjugated anti-CD11c (clone HL3), PE-CF594-conjugated anti-Ly-6C (clone 49-44), FITC-conjugated anti-CD103 (clone M290), PE-conjugated anti-Lamp-1 (CD107a) (clone 1D4B) and PE-conjugated streptavidin antibodies were purchased from BD Biosciences. Anti-mouse PE-conjugated anti-CXCR4 (clone 2B11), anti-mouse PE-conjugated anti-CD49d (clone R1-2) and anti-mouse anti-CD86 biotin (clone GL-1) antibodies were purchased from eBioscience. Anti-mouse PerCP-Cy5.5-conjugated anti-MHC-II (Ia-Ie) (clone M5/M4,15,2) and BV421-conjugated anti-CD64 (clone X54-5/7.1) antibodies were purchased from Biolegend.

Unconjugated goat anti-mouse MPO (catalog no. AF3667) antibodies were purchased from R&D systems; unconjugated rabbit anti-mouse anti-citrullinated H3 (catalog no. Ab5103) antibodies were purchased from Abcam. Donkey anti-rabbit and anti-goat IgG antibodies conjugated with AlexaFluor568 and AlexaFluor488, respectively, were purchased from ThermoFisher.

Anti-mouse HSP90α, goat anti-rabbit immunoglobulins/HRP and rabbit anti-mouse immunoglobulins/HRP were purchased from Agilent.

Additional reagents can be found in the sections below.

Model of low-dose-LPS-triggered allergic asthma to HDM. Isoflurane-anesthetized BALB/c wild-type mice were instilled i.n. with different doses of LPS ranging from 0.1 ng to 10 µg, two of which were chosen as low (100 ng) or high (10 µg) doses (LPS from *Escherichia coli* O55:B5, Sigma-Aldrich). Vehicle mice were instilled i.n. with 50 µl of PBS. One day later (day 1), mice were administered i.n. with 40 µg of HDM (HDM *pteronyssinus*, Greer Laboratories) in 50 µl of PBS. Seven days later (day 8), all mice were challenged by i.n. instillation of 10 µg of HDM in 50 µl of PBS. Three days after the HDM challenge (day 11), we estimated bronchial hyperresponsiveness to methacholine by assessing dynamic airway resistance in anesthetized animals subjected to increased doses of methacholine with a FlexiVent small animal ventilator (SCIREQ) system[42]. Animals were then euthanized, and features of allergic airway inflammation were assessed. BALF cytology and lung histology were performed as described[42]. The extent of perivascular and peribronchial inflammation was estimated by a score calculated by means of quantification of inflammatory cells in lung sections stained with hematoxylin and eosin[35]. Briefly, score 0 was assigned to bronchi with no surrounding leukocyte infiltration; score 1 corresponded to few infiltrating leukocytes; scores 2 or 3 were assigned if there were from 1 to 2 or 3 to 5 layer(s) of perivascular and/or peribronchial leukocytes, respectively. Mucus production was quantified as the percentage of Periodic acid–Schiff (PAS)–stained goblet cells per total epithelial cells in randomly selected bronchi. Bronchial lymph node (BLN) cells were collected, pooled from 2–5 mice (Figs. 1c, 4j, 5d and 8b,g) and cultured in complete RPMI medium with or without HDM restimulation (30 µg ml^{-1}). Culture supernatants were assessed for cytokine production (IL-4, IL-5, IL-13, IFN-γ) by ELISA (eBiosciences).

Cell isolation, staining and flow cytometry. To obtain single-lung-cell suspensions, lungs were perfused with 10 ml of PBS through the right ventricle, cut into small pieces and digested for 1 h at 37 °C in HBSS containing 1 mg ml^{-1} collagenase A (Roche) and 0.05 mg ml^{-1} DNase I (Roche). Blood was collected in an EDTA-containing tube (100 mM), and red blood cells were lysed with red blood cell lysis buffer (eBioscience). BM cells were isolated by flushing femurs with PBS. Cells were filtered through a 70-µM cell strainer to obtain single-cell suspensions.

Cell phenotyping and sorting were performed on a FACSCANTO II and a FACSARIA III (BD Biosciences), respectively. Staining reactions were performed at 4°C with 2% v/v of Fc block (BD Pharmingen) to reduce nonspecific binding. Anti-mouse Lamp-1 intracellular staining was performed with the Foxp3/Transcription factor Staining Buffer Set from eBiosciences.

FSC-W and FSC-A discrimination was used to exclude doublet cells, and ViaProbe (7-AAD) cell viability solution (BD Biosciences) was used to discriminate between dead and living cells. BM, blood and lung neutrophils were identified as SSC^{hi}CD45^{+}CD11b^{hi}Ly-6G^{hi} cells. Neutrophil mean fluorescence intensity (MFI) of specific markers was quantified with FlowJo. Results were analyzed with FlowJo (Tree Star).

For scRNA-seq, adoptive transfer and co-culture experiments, single-lung-cell suspensions were obtained from lungs of vehicle, LPS^{lo} and LPS^{hi} mice 24 h after treatment. Neutrophils were first enriched by negative selection with a MACS Neutrophil Isolation kit (Miltenyi Biotec) and then sorted as CD45^{+} cells with nozzle 100 at 3,000 events s^{-1} (see Supplementary Fig. 2b,c). Trypan blue-treated cells were examined under the microscope for counting and viability testing. Viability was above 95% for all three samples. Cell preparations were centrifuged at 300*g* for 5 min. For scRNA-seq, neutrophils were isolated from lung single-cell suspensions pooled from 3 BALB/c female wild-type mice per condition and were resuspended in calcium- and magnesium-free PBS containing 400 µg ml^{-1} bovine serum albumin (BSA, Sigma-Aldrich).

For cytologic examination and immunofluorescence ex vivo, CD45^{+}CD11b^{hi}Ly-6G^{hi}CD49d^{lo} neutrophils from vehicle and LPS^{hi} mice and CD45^{+}CD11b^{hi}Ly-6G^{hi}CD49d^{hi} neutrophils from LPS^{lo} mice were FACS sorted 24 h after LPS.

ScRNA-seq: library construction with 10x Genomics platform. Cellular suspensions were loaded on the Chromiu Controller (10x Genomics, Pleasanton) to generate Gel Bead-In-EMulsions (GEMs). Barcoded sequencing libraries were generated with the Chromium Single Cell 3′ Reagent Kits v2 (10x Genomics) following manufacturer's instructions. Sequencing libraries were loaded at 1.4 pM on an Illumina NextSeq500 with NextSeq 500/550 Mid Output v2 kit (150 cycles) (Illumina) with the following read lengths: 26 base pairs (bp) for Read 1 (16-bpBarcode + 10-bp Randomer), 8 bp for Sample Index and 58 bp for Read 2.

Analysis scRNA-seq samples. Cell Ranger software (v.1.2.0) (10x Genomics) was used to demultiplex Illumina BCL files to FASTQ files (cellranger mkfastq), to perform alignment (to mouse GRCm38/mm10 genome), filtering, UMI counting and to produce gene–barcode matrices (cellranger count).

Subsequent analysis used R bioconductor[43] (v.3.4.2.) and the R package Seurat[44] (v.2.1.0). We first performed a quality-control analysis and selected cells for further analysis (see Supplementary Fig. 2d,e). Gene counts were normalized, and highly variable genes were calculated. Cell–cell variation in the number of detected UMI was regressed out with the ScaleData function. Linear dimensional reduction was performed on the scaled data with the 'RunPCA' function. To identify the number of statistically significant principal components (PCs) to include for subsequent analyses, we used the 'JackStraw' function, which implements a resampling test inspired by the jackStraw procedure[44]. PCs 1:11 were used in the subsequent analyses. We have also performed analyses including lower and higher numbers of PCs (1:8 to 1:13) and did not find any substantial change in the results obtained. Cells were clustered via the 'FindClusters' function. Several cluster resolutions were tested, and the resolution of 0.25 was chosen, because higher resolutions created additional subdivisions or clusters containing singlets, which were considered not relevant. To visualize the data, nonlinear dimensional reduction was used, and *t*SNE plots were created by use of the 'RunTSNE' function, with the number of dimensions to use set to 11 (PCs 1:11). The aforementioned analyses were performed on the individual Seurat objects (encompassing data from vehicle, LPS^{lo} and LPS^{hi} mice) but also on a merged Seurat object that encompassed merged data from vehicle, LPS^{lo} and LPS^{hi} mice. Differential expression (DE) analysis between clusters was performed with the 'FindMarkers' function. A value of 0.25 was attributed to the min.pct argument, which requires a gene to be detected at least in 25% in either of the two groups of cells. Only DE genes with an adjusted P value $< 10^{-3}$ were retained. To define the transcriptomic signature of steady-state neutrophils (cluster 0) (see Supplementary Fig. 3c,d), lists of the significantly upregulated genes in cluster 0 compared to cluster 1 (that is, LPS^{lo}-induced), cluster 0 compared to clusters 2, 3 and 5 (that is, LPS^{hi}-induced), and cluster 0 compared to cluster 4 were generated, and genes commonly found in each of the 3 lists were retained. To define the common 'LPS signature' (see Supplementary Fig. 3e,f), lists of the significantly upregulated genes in cluster 1 compared to cluster 0, clusters 2, 3 and 5 compared to 0, and cluster 4 compared to cluster 0 were generated, and genes commonly found in each of the 3 lists were retained. To define cluster-specific gene signatures, only genes that did not belong to the common LPS signature and that were significantly upregulated in that specific cluster as compared to each of the others were retained. Statistical enrichment tests for Gene Ontology (GO) biological processes were performed with PANTHER 13.1 using a specific gene set for each cluster with a P value $<10^{-3}$ and minimal detection in 25% of cells with all genes contained in GO's *Mus musculus* database as reference.

Neutrophil cytologic examination. Cytologic examination of FACS-sorted neutrophils was performed on cytospin preparations stained with Hemacolor (Merck KgaA). Sections were examined with a FSX100 microscope (Olympus). Quantifications of neutrophil size and cytoplasm/nucleus ratio were performed with the ImageJ software.

Immunofluorescence. To assess the ability of neutrophils to form NETs ex vivo, 2.5×10^5 FACS-sorted neutrophils were seeded and cultured ex vivo on slides (Nunc Lab-Tek II Chamber Slide system, Sigma) precoated with poly-D-lysin hydrobromide (Sigma) for 24 h in supplemented D-MEM medium (Gibco). Supernatants were removed and chambers were rinsed with PBS. Slides were

then fixed with paraformaldehyde 10%, rinsed twice with PBS and permeabilized in PBS 0.5% triton X-100. Slides were then blocked and stained as described below.

To identify NETs from lung tissues, lungs were collected without performing BALF and fixed with 4% paraformaldehyde in PBS. Lung tissues were paraffin-embedded, and lung sections were cut (2-µm-thick sections) for immunofluorescence staining. After deparaffinization and rehydration, tissue sections were boiled for 20 min in 10-mM sodium carbonate buffer for antigen retrieval. Lung sections were permeabilized in PBS 0.5% triton X-100.

Samples were incubated with a blocking buffer (PBS with 2% BSA and 2% of donkey serum (Sigma-Aldrich)) for 1 h at room temperature (RT) and stained in blocking buffer with rabbit anti-mouse antibodies directed against citrullinated histone H3 (1:100 in blocking buffer) and with goat anti-mouse antibodies directed against MPO (1:40 in blocking buffer) during 1 h at RT. After washing samples with PBS, secondary donkey anti-rabbit IgG antibodies conjugated with AlexaFluor568 (1:200 in blocking buffer) and donkey anti-goat IgG antibodies conjugated with AlexaFluor488 (1:200 in blocking buffer) were added in blocking buffer containing DAPI (1:1,000) and incubated for 2 h in the dark at RT. Finally, samples were mounted with 10 µl of ProLong Antifade reagent (ThermoFisher) on glass slides and stored at RT in the dark overnight.

All samples were analyzed by fluorescence microscopy with standard filter sets. Controls were stained with secondary antibody only, and nonspecific fluorescent staining was not detected when secondary antibodies were tested alone. Images were acquired on a Zeiss LSM 880 Airyscan Elyra S.1. confocal microscope (Zeiss) and processed with the ImageJ software. To quantify the volume of NETs released by neutrophils ex vivo (see Supplementary Fig. 4g) or present in the lung tissue (see Figs. 3j,k, 5a,b and 7i,m and Supplementary Figs. 5g, 6b and 7j), Z stack pictures were acquired and Imaris software was used. Briefly, we performed a three-dimensional reconstruction of structures staining double positive for H3-Cit (red) and MPO (green), and Imaris provided quantification of the volume of these structures, expressed as mm^3 per 10^2 neutrophils for ex vivo experiments (counted under the bright-field microscope and staining positive for intracellular MPO associated with the granules) or per 10^2 mm^3 of lung tissue.

DsDNA measurement in BALF. DsDNA was measured in the acellular fraction of the BALF, which was obtained after a double centrifugation and supernatant collection. Levels of dsDNA were determined withQuant-iT PicoGreen dsDNA reagent (Invitrogen) according to the manufacturer's protocol.

Western blotting. Lung tissues were homogenized in RIPA buffer supplemented with a cocktail of protease inhibitors (Complete, Roche). An equivalent amount of protein per sample was resolved on a 4–20% gel (Mini-PROTEAN TGX Precast Gels, biorad) and electroblotted on Invitrolon PVDF membranes (Life Technologies). Membranes were blocked 1 h at RT in TBS-Tween 0.1% containing 5% of dry milk and incubated overnight at 4 °C with primary antibody anti-citrullinated H3 (1:1,000 in 0.1% TBS-tween and 5% BSA). The membranes were then incubated 2 h at RT with appropriate HRP-associated secondary antibodies in TBS-tween 0.1% containing 5% BSA. Equal loading was confirmed by probing for HSP90α.

Measurement of NE–DNA complexes in BALF. Nunc plates (ThermoFisher) were coated overnight with anti-neutrophil elastase antibodies (1:2,000, Abcam, ab21595) and washed 3 times with PBS-Tween 0.05%. Plates were blocked 1 h at RT with PBS-BSA 1% and washed 3 times. Samples were then loaded for 2 h at RT and plates were then washed 5 times. Mouse anti-dsDNA antibodies were added for 1 h at RT followed, after 5 washes, by incubation with biotinylated rat anti-mouse IgG polyclonal antibodies for 90 min at RT. After extensive washing, secondary streptavidin-HRP (BD pharmingen, catalog no. 554066) was added for 30 min at RT, followed by 5 washes. The relative amount of NE–DNA complexes was revealed with TMB substrate solution (Sigma-Aldrich).

Antibody-mediated neutrophil in vivo depletion. Neutrophils were depleted by i.p. injection of 500 µg of anti-Ly-6G antibody (InVivo Plus anti-mouse Ly-6G, clone 1A8, Bioxcell) intraperitoneally (i.p.) 1 d before (day –1), at day 0 and 1 d after LPS exposure (day 1) (see Supplementary Fig. 5a). Mice were killed 3 h later.

Inhibition of LPS-induced lung neutrophil recruitment. To inhibit LPS-induced lung neutrophil recruitment[28], an antagonist of the chemokine receptor CXCR2 (that is, Sch527123[27], MedChem Express) was given orally, by gavage, at the dose of 3 mg kg^{-1}, 2 h before, 4 h after and 8 h after LPS treatment, as well as 2 h before and 4 h after i.n. administration of 40 µg of HDM. Seven days later, mice were challenged with 10 µg of HDM, and features of allergic airway inflammation were assessed 3 d later.

Neutrophil adoptive transfers. After MACS enrichment and FACS sorting, neutrophils were resuspended in calcium- and magnesium-free PBS at the concentration of 2.10^7 cells/ml. Five hundred thousand (5×10^5) cells, together with 40 µg of HDM, were injected intratracheally to naive mice in 50 µl of PBS. Seven days later, mice were challenged with 10 µg of HDM, and features of allergic airway inflammation were assessed 3 d later.

Degradation of NETs and inhibition of NET formation in vivo. The formation of NETs was prevented in vivo by i.p. injection of NEi (GW-311616 hydrochloride, Axon Medchem) (2.5 µg g^{-1} in 200 µl of PBS) or of Cl-amidine (10x stock solution in DMSO, Sanbio) (10 mg kg^{-1} in 200 µl of 1% DMSO v/v in PBS), twice daily from day –1 to day +2 (LPS model) or from day 5 to day 17 (PR8 infection model), or from day 0 to day 3 (ozone model). Alternatively, NETs were degraded by injecting 1,000 IU DNase I (Sigma-Aldrich) i.p. in 200 µl of HBSS once daily from day –1 to day +2 (model of LPS exposure) or from day 5 to day 17 (PR8 infection model) or from day 0 to day 3 (ozone model). In pilot experiments, we compared the responses of LPS^{lo}-HDM, PR8-HDM or ozone-HDM mice with their vehicle-treated counterparts (either HBSS, PBS or 1% DMSO v/v, used separately) and confirmed that vehicle did not affect the response. In subsequent experiments, vehicle LPS^{lo}-HDM, PR8-HDM or ozone-HDM mice were treated randomly with either HBSS, PBS or DMSO 1% v/v.

AF647-HDM uptake by lung DC subsets. To assess HDM uptake by lung DCs, LPS^{lo} or ozone-exposed mice were administered i.n. with 40 µg of HDM labeled with Alexafluor-647 (AF647-HDM) (Alexa Fluor 647 Protein Labeling Kit, ThermoFisher) 24 h after treatment. Alternatively, PR8-infected mice were injected i.n. with AF647-HDM at day 7 after infection. Twenty-four hours later, lung-single-cell suspensions were obtained, and lung DCs were selected as $CD45^+CD3e^-CD19^-SiglecF^-Ly\text{-}6G^-NK1.1^-MHC\text{-}II^+CD11c^+$ cells and were then subdivided into $CD11b^-CD103^+$, $CD11b^+Ly\text{-}6C^-$ and $CD11b^+Ly\text{-}6C^+$ subsets by flow cytometry (see Fig. 6a). Alternatively, mice were also treated with NEi, Cl-amidine or DNase as described above.

Neutrophils/BMDCs co-culture experiments. To generate BMDCs, BM cells were isolated from naive BALB/c mice and were grown for 7 d in GM-CSF-containing medium, as described[33]. Vehicle, LPS^{lo} and LPS^{hi} neutrophils were isolated 24 h after treatment. In total, 2.5×10^5 neutrophils were seeded into 48-well plates previously coated with poly-D-lysin hydrobromide (Sigma) in supplemented D-MEM medium (Gibco) and allowed to adhere for 2 h. BMDCs were then added to neutrophil cultures at a ratio of 1:1. Finally, AF647-HDM (500 ng ml^{-1}) and DNase I (400 IU ml^{-1}, Sigma-Aldrich) were added to the culture. Twelve hours later, cells were collected, washed, resuspended in FACS medium and stained for flow cytometry analysis.

Influenza A virus infection protocol. Influenza A virus strain A/PR8/34 (H1N1) was kindly provided by F. Trottein (Institut Pasteur). The viral stock suspension (10^8 PFU ml^{-1}) was diluted, and 5 PFU were administered i.n. to isoflurane-anesthetized mice in 50 µl of PBS.

Assessment of viral mRNA expression. Lung apical lobes were excised, and total mRNA was isolated from homogenized tissue according to the Immgen protocol (www.immgen.org). cDNA was obtained with RevertAid First Strand cDNA Synthesis Kit (ThermoFisher Scientific), and qPCR was performed in duplicate with iTaq Universal SYBR geen supermix (Biorad) and ABI 7900HT Fast Real-Time PCR System (Applied Biosystems). Primer sequences were as follows: 5′-TTCACCATTGCCTTCTCTTC-3′ and 5′-CCCATTCTCATTACTGCTTC-3′ for viral NS1, 5′-AGCCCAGTGTTACCACCAAG-3′ and 5′-ACCCAAGAACAA GCACAAGG-3′ for housekeeping gene *Ubc*, 5′-TGGCAAAGTGGAGATTGTTG CC-3′ and 5′-AAGATGGTGATGGGCTTCCCG-3′ for housekeeping gene *Gapdh*, 5′-CATGGCTCGCTCGGTGACC-3′ and 5′-AATGTGAGGCGGG TGGAACTG-3′ for housekeeping gene *B2m*. Expression levels of NS1 were normalized relative to the three control genes (*Ubc, B2m* and *Gapdh*).

Model of PR8-triggered allergic asthma to HDM. Seven days after infection, mice were administered i.n. with 40 µg of HDM. Seven days later (day 7), all mice were challenged by i.n. instillation of 10 µg of HDM. Three days after the challenge, animals were killed and features of allergic airway inflammation were assessed, as described above. In addition, levels of HDM-specific IgG1 were quantified, as described[20].

Model of ozone-triggered allergic asthma to HDM. Naive mice were exposed for 3 consecutive days to 2 ppm ozone during 3 h. Twenty-four hours after the last ozone exposure, mice were administered i.n. with 40 µg of HDM. Seven days later, mice were challenged with 10 µg of HDM, and features of allergic airway inflammation were assessed 3 d later as described above.

Statistical analysis. Respect of the assumptions of normal distribution of residuals and homoscedasticity was verified, and data were presented as mean + s.e.m., as well as individual values, unless otherwise indicated. Data from independent experiments were pooled for analysis in each data panel, unless otherwise indicated. Statistical analyses were performed with Prism 6 (GraphPad Software). We considered a *P* value lower than 0.05 as significant.

Reporting Summary. Further information on research design is available in the Nature Research Reporting Summary linked to this article.

Data availability

The scRNA-seq data provided in this manuscript have been deposited in the ArrayExpress database at EMBL-EBI (https://www.ebi.ac.uk/arrayexpress/experiments/E-MTAB-6902) under accession number E-MTAB-6902. The figures that have associated scRNA-seq data are the following: Fig. 2, Supplementary Figs. 2 and 3. The source data underlying Fig. 1a–d,f, 2d, 3b,c,f,g,i,k, 4b–e,g,i–k,m, 5b–e,g, 6b,d,f, 7b–i,k–m and 8a–c,e,f–h,j and Supplementary Figs. 1b,d, 4c,d, 5b,c,e,g, 6b, 7b–d,f,g,i,j and 8a are provided as a Source Data file. Any data that support the findings of this study are available from the corresponding authors upon request.

References

42. Sabatel, C. et al. Exposure to bacterial CpG DNA protects from airway allergic inflammation by expanding regulatory lung interstitial macrophages. *Immunity* **46**, 457–473 (2017).
43. Gentleman, R. C. et al. Bioconductor: open software development for computational biology and bioinformatics. *Genome Biol.* **5**, R80 (2004).
44. Macosko, E. Z. et al. Highly parallel genome-wide expression profiling of individual cells using nanoliter droplets. *Cell* **161**, 1202–1214 (2015).

nature research

Corresponding author(s): Thomas MARICHAL, Fabrice BUREAU

Last updated by author(s): Aug 12, 2019

Reporting Summary

Nature Research wishes to improve the reproducibility of the work that we publish. This form provides structure for consistency and transparency in reporting. For further information on Nature Research policies, see Authors & Referees and the Editorial Policy Checklist.

Statistics

For all statistical analyses, confirm that the following items are present in the figure legend, table legend, main text, or Methods section.

n/a	Confirmed	
☐	☒	The exact sample size (*n*) for each experimental group/condition, given as a discrete number and unit of measurement
☐	☒	A statement on whether measurements were taken from distinct samples or whether the same sample was measured repeatedly
☐	☒	The statistical test(s) used AND whether they are one- or two-sided *Only common tests should be described solely by name; describe more complex techniques in the Methods section.*
☒	☐	A description of all covariates tested
☐	☒	A description of any assumptions or corrections, such as tests of normality and adjustment for multiple comparisons
☐	☒	A full description of the statistical parameters including central tendency (e.g. means) or other basic estimates (e.g. regression coefficient) AND variation (e.g. standard deviation) or associated estimates of uncertainty (e.g. confidence intervals)
☐	☒	For null hypothesis testing, the test statistic (e.g. *F*, *t*, *r*) with confidence intervals, effect sizes, degrees of freedom and *P* value noted *Give P values as exact values whenever suitable.*
☒	☐	For Bayesian analysis, information on the choice of priors and Markov chain Monte Carlo settings
☒	☐	For hierarchical and complex designs, identification of the appropriate level for tests and full reporting of outcomes
☒	☐	Estimates of effect sizes (e.g. Cohen's *d*, Pearson's *r*), indicating how they were calculated

Our web collection on statistics for biologists contains articles on many of the points above.

Software and code

Policy information about availability of computer code

Data collection	Cell Ranger software (v1.2.0) (10x Genomics) was used to demultiplex Illumina BCL files to FASTQ files (cellranger mkfastq), to perform alignment (to mouse GRCm38/mm10 genome), filtering, UMI counting and to produce gene – barcode matrices (cellranger count).
Data analysis	Single cell analysis used R bioconductor (version 3.4.2.), and the R package Seurat (version 2.1.0). Statistical enrichment tests for GO biological processes were performed with PANTHER 13.1. Flow cytometry analysis were performed with FlowJo (version 10.1, Tree Star, Ashland, USA). Immunofluorescence images were acquired on a Zeiss LSM 880 Airyscan Elyra S.1. confocal microscope (Zeiss) and analyzed using the ImageJ (version 15.1n) and Imaris (version 7.5.2) softwares. Statistics: GraphPad Prism 6 for PC, R Bioconductor.

For manuscripts utilizing custom algorithms or software that are central to the research but not yet described in published literature, software must be made available to editors/reviewers. We strongly encourage code deposition in a community repository (e.g. GitHub). See the Nature Research guidelines for submitting code & software for further information.

Data

Policy information about availability of data

All manuscripts must include a data availability statement. This statement should provide the following information, where applicable:

- Accession codes, unique identifiers, or web links for publicly available datasets
- A list of figures that have associated raw data
- A description of any restrictions on data availability

The scRNA-seq data provided in this manuscript have been deposited in the ArrayExpress database at EMBL-EBI (https://www.ebi.ac.uk/arrayexpress/experiments/E-MTAB-6902) under accession number E-MTAB-6902. The figures that have associated raw data are the following: Fig. 2, Supplementary Figs. 2,3.

Field-specific reporting

Please select the one below that is the best fit for your research. If you are not sure, read the appropriate sections before making your selection.

☒ Life sciences ☐ Behavioural & social sciences ☐ Ecological, evolutionary & environmental sciences

For a reference copy of the document with all sections, see nature.com/documents/nr-reporting-summary-flat.pdf

Life sciences study design

All studies must disclose on these points even when the disclosure is negative.

Sample size	We assume that variance will be equal between experimental groups. We estimate that a difference will be biologically significant between two groups if a variation of at least 50% is observed between the mean of the two groups. If we want to compare two means of 1500 and 3000 with a standard deviation of 750 (example from the number of eosinophils in the bronchoalveolar lavage fluid of asthmatics and controls mice) , the results of power analysis for expecting effects show that for a power of 0.9 (and $\alpha<0.05$) in a t student test, the required sample size would be 3-5 animals. In most of the experiments, 3 to 10 mice/group was sufficient to identify differences between groups with at least 90% power and a 5% significance level.
Data exclusions	No data was excluded from the analyses.
Replication	For each experiment, each experimental group was composed of 3-5 mice constituting biological replicates. Each experiments have been repeated two to four times. All attempts at replication were successful and gave similar readout.
Randomization	Female age-matched BALB/c mice were randomly allocated into experimental groups.
Blinding	Blinding was only relevant for histological analysis of H&E and PAS stained-lung sections. All other conclusions were made based on quantitative parameters and statistical significance.

Reporting for specific materials, systems and methods

We require information from authors about some types of materials, experimental systems and methods used in many studies. Here, indicate whether each material, system or method listed is relevant to your study. If you are not sure if a list item applies to your research, read the appropriate section before selecting a response.

Materials & experimental systems

n/a	Involved in the study
☐	☒ Antibodies
☒	☐ Eukaryotic cell lines
☒	☐ Palaeontology
☐	☒ Animals and other organisms
☒	☐ Human research participants
☒	☐ Clinical data

Methods

n/a	Involved in the study
☒	☐ ChIP-seq
☐	☒ Flow cytometry
☒	☐ MRI-based neuroimaging

Antibodies

Antibodies used	Anti-mouse FITC-, and V500-conjugated anti-CD45.2 (clone 104, dilution 1/100, #561874, #562130), PE-conjugated anti-CD3 (clone 142-2C11, dilution 1/100, #553064), PE-conjugated anti-CD19 (clone 1D3, dilution 1/300, #553786), PE-conjugated anti-NK1.1 (clone pk136, dilution 1/300, # 553165), PE-conjugated anti-Siglec-F (clone E50-2440, dilution 1/500,#552126), PE-conjugated anit-Ly6G (clone 1A8, dilution 1/500, #551461), eFluor450- and PE-Cy7-conjugated anti-CD11b (clone M1/70, dilution 1/300, #560455, #561098), PE-Cy7-conjugated anti-Ly6G (clone 1A8, dilution 1/200, #560501), APC-Cy7-conjugated anti-CD11c (clone HL3, dilution 1/150, #561241), PE-CF594-conjugated anti-Ly6C (clone 49-44, dilution 1/200, #562728), FITC-conjugated anti-CD103 (clone M290, dilution 1/100, #557494) and PE-conjugated anti-Lamp-1 (CD107a) (clone 1D4B, dilution 1/100, #558661), Anti-mouse PE-conjugated anti-CXCR4 (clone 2B11, dilution 1/100, #561734) antibodies were purchased from BD biosciences. Anti-mouse PE-conjugated anti-CD49d (clone R1-2, dilution 1/100, #12-0492-81) antibodies were purchased from eBioscience. Anti-mouse PerCP-Cy5.5-conjugated anti-MHC-II (Ia-Ie) (clone M5/M4,15,2, dilution 1/1000, #107626) and BV421-conjugated anti-CD64 (clone X54-5/7.1, dilution 1/100, #139309) antibodies were purchased from Biolegend. Unconjugated Goat anti-myeloperoxydase (dilution 1/40, #AF3667) was purchased from R&D systems and unconjugated rabbit anti-histone H3 citrullinated (dilution 1/100, #ab5103) was purchased from abcam.
Validation	All the antibodies are from commercial sources and purhcased from BD pharmingen, Ebioscience, biolegend, R&D systems and abcam. The data sheets were provided by the manufacturer, in which the validation of antibodies for the specificity to the mouse antigen and for the usage for flow cytometry/western blot/confocal microscopy was confirmed. Statements about validation are found in manufacturer's website.

Animals and other organisms

Policy information about studies involving animals; ARRIVE guidelines recommended for reporting animal research

Laboratory animals	Mus musculus, BALB/c, female, 6 to 10 weeks
Wild animals	The study did not involve wild animals.
Field-collected samples	The study did not involve samples collected from the field.
Ethics oversight	All animal experiments described in this study were reviewed and approved by the Institutional Animal Care and Use Committee of the University of Liège. The "Guide for the Care and Use of Laboratory Animals", prepared by the Institute of Laboratory Animal Resources, National Research Council, and published by the National Academy Press, as well as European and local legislations, were followed carefully.

Note that full information on the approval of the study protocol must also be provided in the manuscript.

Flow Cytometry

Plots

Confirm that:

☒ The axis labels state the marker and fluorochrome used (e.g. CD4-FITC).

☒ The axis scales are clearly visible. Include numbers along axes only for bottom left plot of group (a 'group' is an analysis of identical markers).

☒ All plots are contour plots with outliers or pseudocolor plots.

☒ A numerical value for number of cells or percentage (with statistics) is provided.

Methodology

Sample preparation	To obtain single-lung-cell suspensions, lungs were perfused with 10 ml of PBS through the right ventricle, cut into small pieces, and digested for 1 h at 37°C in HBSS containing 1 mg/ml collagenase A (Roche) and 0.05 mg/ml DNase I (Roche). Blood was collected in an EDTA-containing tube (100 mM), and red blood cells were lysed with RBC lysis buffer (eBioscience). BM cells were isolated by flushing femurs with PBS.Staining reactions were performed at 4°C after incubation with 2.4G2 Fc receptor blocking antibodies to avoid non-specific binding. Anti-mouse Lamp-1 intracellular staining was performed using the Foxp3/Transcription factor Staining Buffer Set from eBiosciences according to the manufacturer's instructions. Briefly, after extracellular staining, cells were resuspended in 200 µl of Fix/Perm buffer for 45 minutes at 4°C in the dark and then washed with 200 µl of permeabilization buffer. Cells were then stained for intracellular protein in permeabilization buffer for 35-40 minutes.
Instrument	Cell phenotyping and sorting were performed on a FACSCANTO II and a FACSARIA III (BD Biosciences), respectively.
Software	FlowJo (version 10.1, Tree Star, Ashland, USA)
Cell population abundance	Purity was between 90 and 95% and was determined by flow cytometry after sorting.
Gating strategy	Lung dendritic cells (DCs) were selected as CD45+CD3e-CD19-Siglec-F-Ly6G-NK1.1-MHCII+CD11c+ cells and were then subdivided into CD11b-CD103+, CD11b+Ly-6C- and CD11b+Ly-6C+ subsets ; lung neutrophils were selected as SSChighCD45.2 +CD11bhighLy-6Ghigh cells. Bone marrow dendritic cells (BMDCs) were selected as MHC-II+CD11c+ cells and further divided between CD11b+Ly-6C+ and CD11b+Ly-6C- subsets.

☒ Tick this box to confirm that a figure exemplifying the gating strategy is provided in the Supplementary Information.

nature immunology

SUPPLEMENTARY INFORMATION

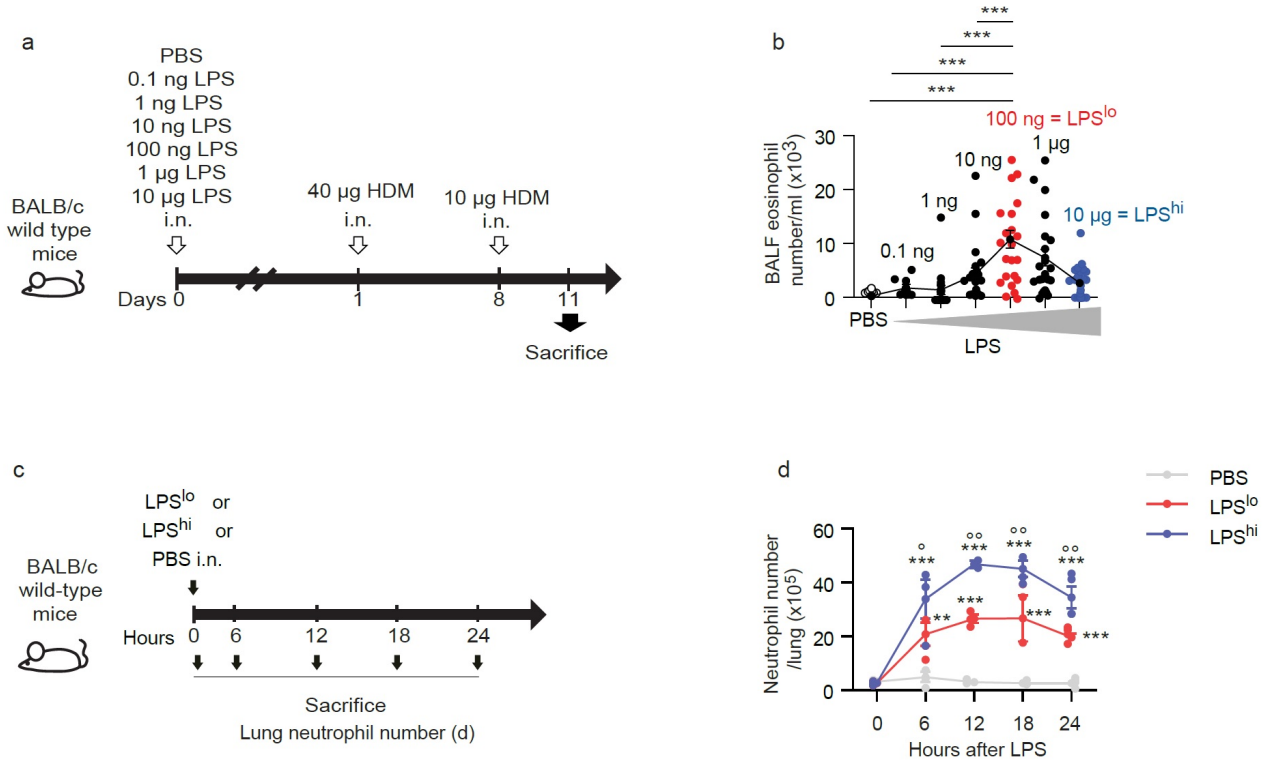
https://doi.org/10.1038/s41590-019-0496-9

In the format provided by the authors and unedited.

Locally instructed CXCR4^{hi} neutrophils trigger environment-driven allergic asthma through the release of neutrophil extracellular traps

Coraline Radermecker[1,2,3,9], Catherine Sabatel[1,3,9], Céline Vanwinge[4], Cecilia Ruscitti[2,3], Pauline Maréchal[2,3], Fabienne Perin[4], Joey Schyns[1,2,3], Natacha Rocks[4], Marie Toussaint[5,6], Didier Cataldo[4], Sebastian L Johnston[5,6,7], Fabrice Bureau[1,3,8,10]* and Thomas Marichal[1,2,3,8,10]*

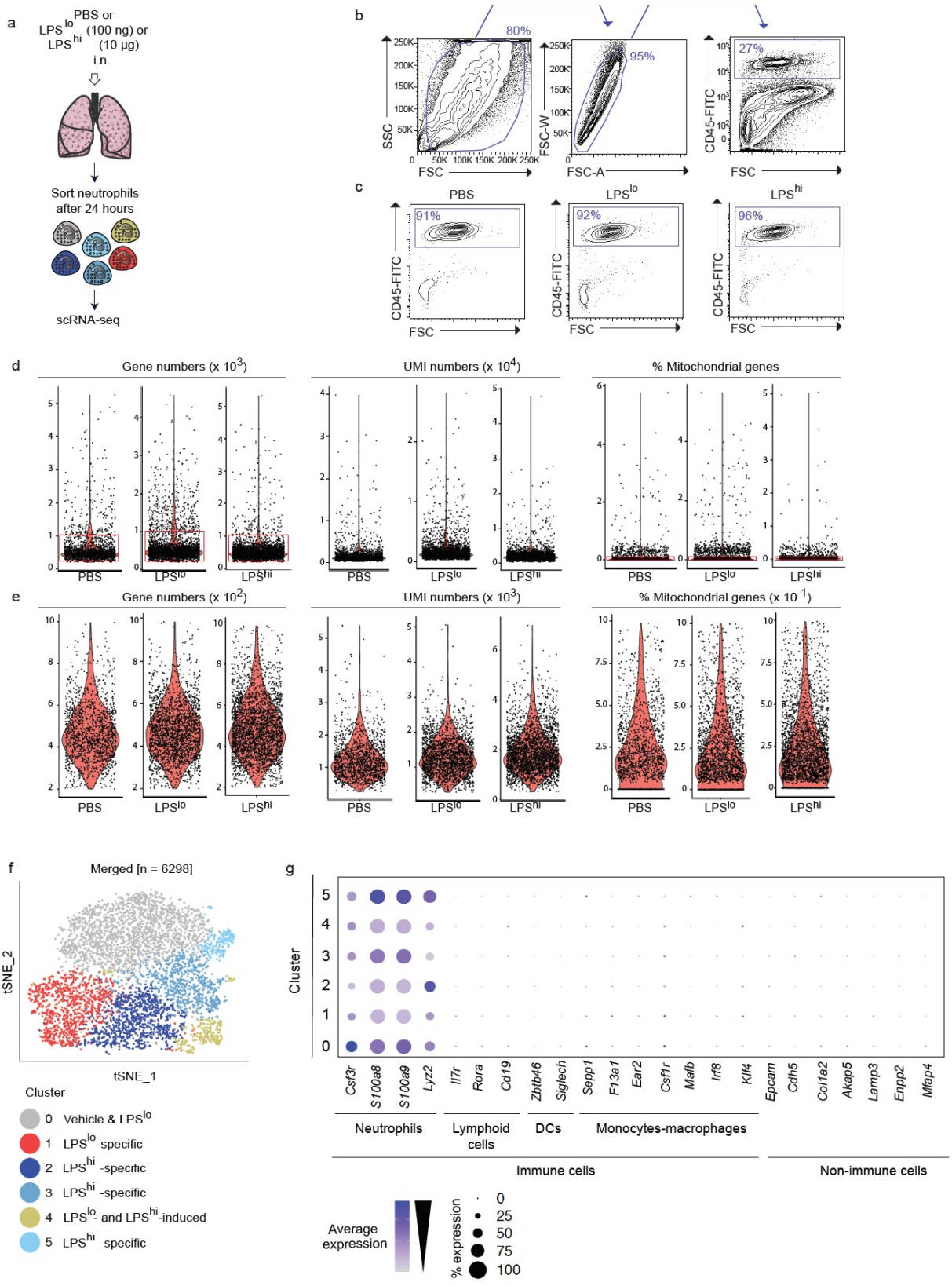
[1]Laboratory of Cellular and Molecular Immunology, GIGA Institute, Liege University, Liege, Belgium. [2]Laboratory of Immunophysiology, GIGA Institute, Liege University, Liege, Belgium. [3]Faculty of Veterinary Medicine, Liege University, Liege, Belgium. [4]Laboratory of Tumor and Development Biology, GIGA Institute, Liege University, Liege, Belgium. [5]Airway Disease Section, National Heart and Lung Institute, Imperial College London, London, UK. [6]Medical Research Council and Asthma UK Centre in Allergic Mechanisms of Asthma, London, UK. [7]Imperial College Healthcare National Health Service Trust, London, UK. [8]Walloon Excellence in Life Sciences and Biotechnology, Wallonia, Belgium. [9]These authors contributed equally: Coraline Radermecker, Catherine Sabatel. [10]These authors jointly supervised this work: Fabrice Bureau, Thomas Marichal. *e-mail: fabrice.bureau@uliege.be; t.marichal@uliege.be



Supplementary Figure 1

BALB/c wild-type mice administered i.n. with different LPS doses exhibit distinct profiles of innate neutrophil recruitment and HDM-induced airway eosinophilia

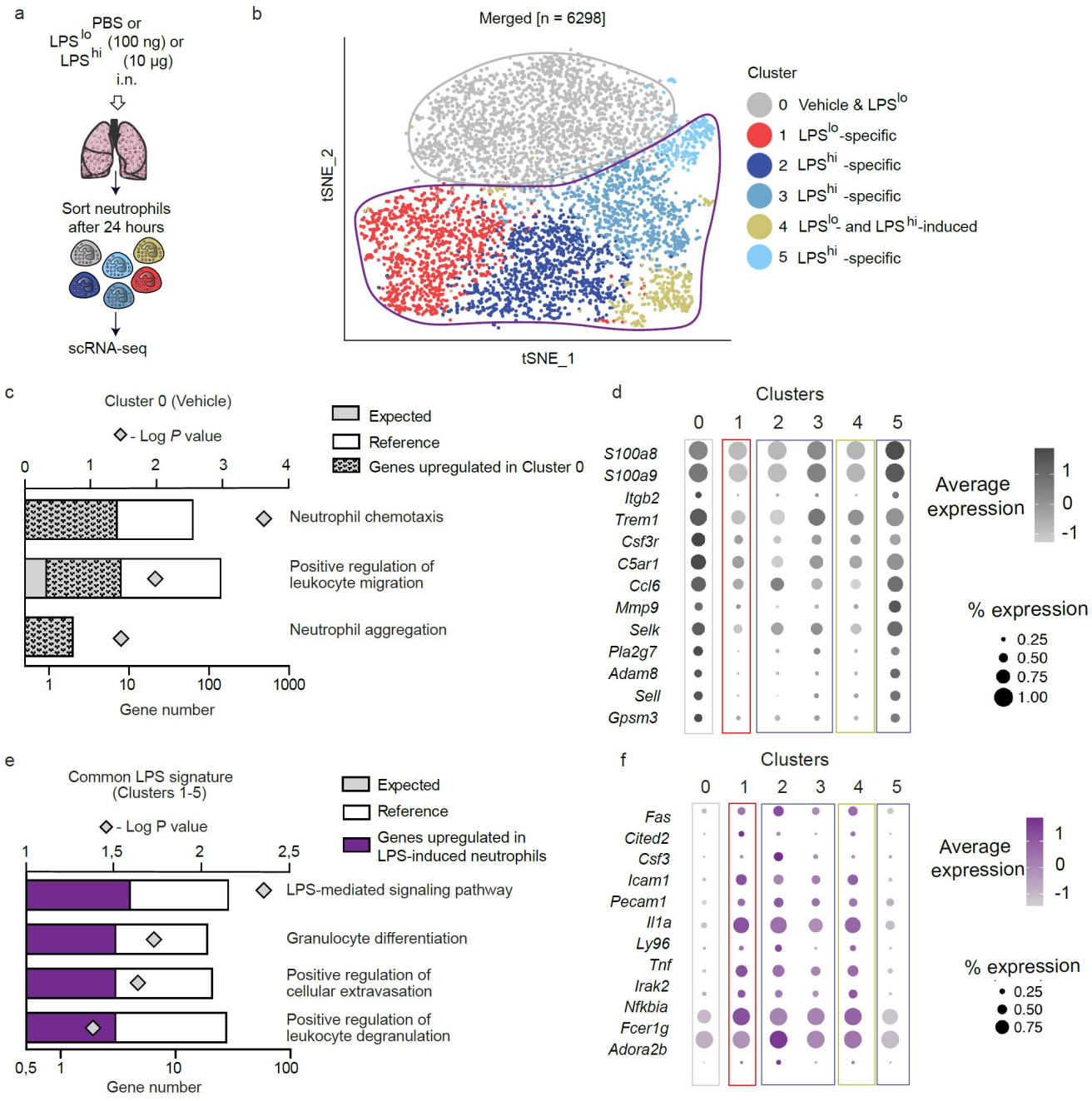
a, Experimental outline for panel **b**. **b**, Eosinophil cell counts in the broncho-alveolar lavage fluid (BALF), assessed 3 d after the second HDM administration in mice exposed to different doses of LPS, ranging from 0.1 ng to 10 µg and instilled i.n. with 40 and 10 µg HDM, 1 and 8 d later, respectively. Data shown are mean +/– s.e.m and are pooled from 4 independent experiments (PBS; LPS 0.1 ng; 1 ng; 10 ng; 100 ng; 1 µg; 10 µg: n = 9;16;22;20;23;24;25 mice per group, respectively). **c**, Experimental outline for panel **d**. **d**, Absolute numbers of lung $CD45^{+}CD11b^{hi}Ly\text{-}6G^{hi}$ neutrophils assessed over time after i.n. vehicle, low-dose LPS (LPS^{lo}) or high-dose LPS (LPS^{hi}) exposure. Data show mean +/– s.e.m. and are pooled from 2 independent experiments (n = 3 [PBS, LPS^{lo}] or 4 [LPS^{hi}] mice per group). P values were calculated using (**b**) a one-way or (**d**) a two-way ANOVA with Tukey's *post hoc* test. In **d**, the symbol * compares the indicated group vs. PBS; the symbol ° compares LPS^{lo} vs. LPS^{hi} groups. °$P < 0.05$; **/°°$P < 0.01$; ***$P < 0.001$. i.n., intranasal.


a
PBS or
LPS^lo (100 ng) or
LPS^hi (10 µg)
i.n.
Sort neutrophils
after 24 hours
scRNA-seq
b
80%
95%
27%
SSC
FSC
FSC-W
FSC-A
CD45-FITC
c
PBS
LPS^lo
LPS^hi
91%
92%
96%
d
Gene numbers (x 10^3)
UMI numbers (x 10^4)
% Mitochondrial genes
e
Gene numbers (x 10^2)
UMI numbers (x 10^3)
% Mitochondrial genes (x 10^-1)
f
Merged [n = 6298]
tSNE_2
tSNE_1
Cluster
0 Vehicle & LPS^lo
1 LPS^lo-specific
2 LPS^hi -specific
3 LPS^hi -specific
4 LPS^lo- and LPS^hi-induced
5 LPS^hi -specific
g
Cluster
Csf3r
S100a8
S100a9
Lyz2
Il7r
Rora
Cd19
Zbtb46
Siglech
Sepp1
F13a1
Ear2
Csf1r
Mafb
Irf8
Klf4
Epcam
Cdh5
Col1a2
Akap5
Lamp3
Enpp2
Mfap4
Neutrophils
Lymphoid cells
DCs
Monocytes-macrophages
Immune cells
Non-immune cells
Average expression
% expression
0
25
50
75
100

Supplementary Figure 2

Lung neutrophils from vehicle, LPS^{lo} and LPS^{hi} mice were isolated and subjected to droplet-based scRNA-seq and quality control filtering and analysis.

a, Simplified experimental outline for scRNA-seq analysis. **b**, Representative FACS sorting strategy of CD45^{+} cells after MACS neutrophil enrichment of lung single-cell suspensions (*n* = 3 pooled mice per group). One PBS-injected mouse is shown. **c**, Post-sort purity of FACS-sorted CD45^{+} cells from vehicle, LPS^{lo} and LPS^{hi} mice 24 h after treatment. Representative post-sort flow cytometry dot plots are shown. Insets indicate the percentage of cells within the indicated gate. **d**,**e**, Gene numbers (left), Unique Molecular Identifiers (UMI) numbers (middle) and percentage of mitochondrial genes (right) detected in vehicle, LPS^{lo} and LPS^{hi} neutrophils before (**d**) and after (**e**) selection and filtering, presented as violin plots (height: gene numbers [left], UMI numbers [middle] and percentage of mitochondrial genes [right]; width: abundance of cells) and individual dots representing individual cells. The red frames indicate cells that were selected for downstream analyses. **f**, *t*SNE plots depicting the transcriptional identity of neutrophils merged from vehicle, LPS^{lo} and LPS^{hi} mice 24 h after treatment, analyzed by scRNA-seq. **g**, Dot plots showing average expression of the indicated genes and percentage of cells expressing the indicated genes within each cluster. High expression of *S100a8*, *S100a9* and *Csf3r* identified the 6 clusters as neutrophils, which was further supported by the virtual absence of expression of markers of other cell types.

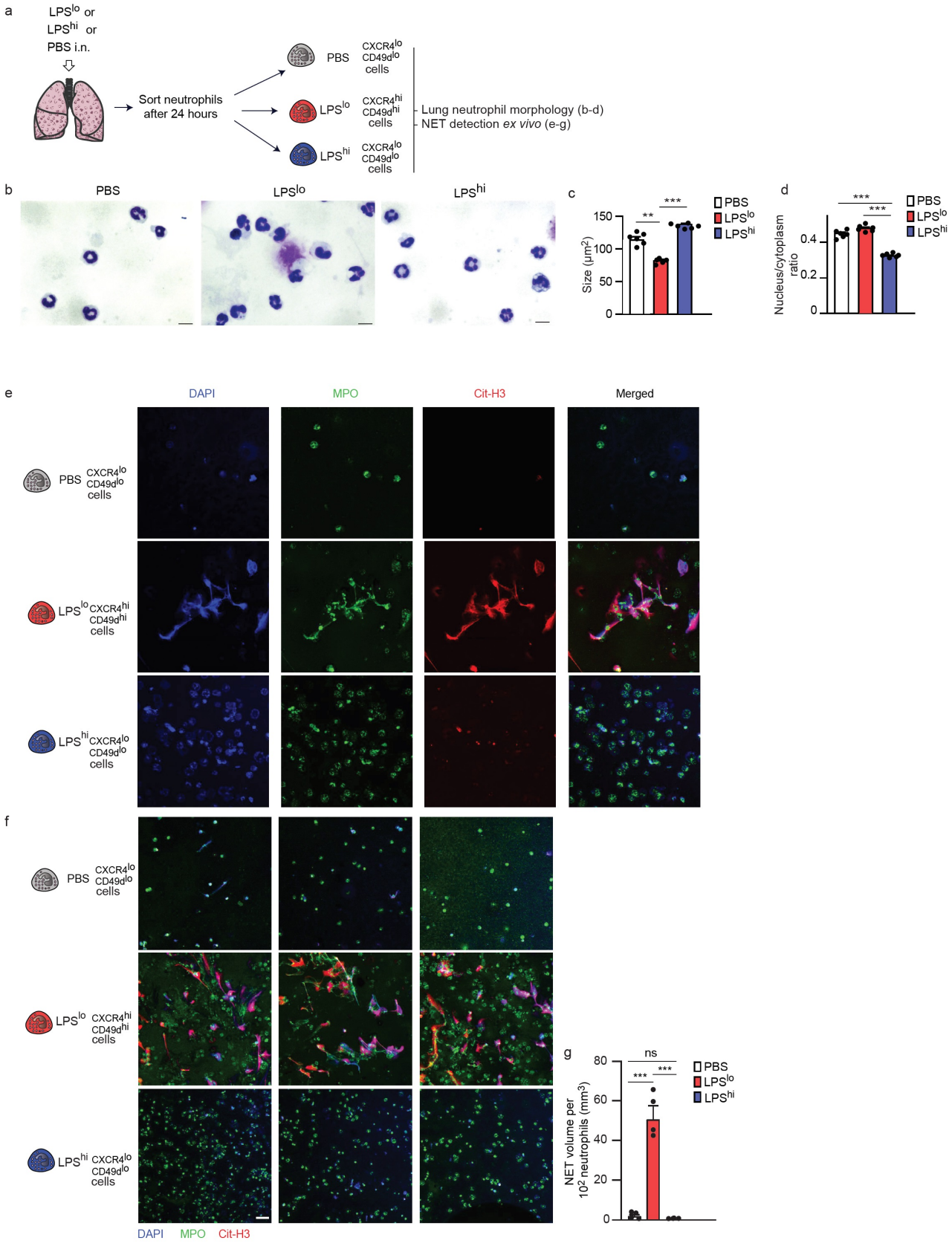


Supplementary Figure 3

Clusters identified by scRNA-seq were analyzed for differential gene expression

a, Simplified experimental outline for scRNA-seq analysis. **b,** *t*SNE plots depicting the transcriptional identity of neutrophils merged from vehicle, LPS^{lo} and LPS^{hi} mice 24 h after treatment, analyzed by scRNA-seq (*n* = 3 pooled mice/condition). **c**, PANTHER GO statistical enrichment tests on the genes significantly upregulated in cluster 0 as compared to the other clusters. **d**, Dot plots showing average expression of the indicated genes and percentage of cells expressing the indicated genes within neutrophil clusters. Depicted genes belong to the lists of genes characterizing the biological responses shown in **c**. **e**, PANTHER GO statistical enrichment tests on the common LPS signature. **f**, Dot plots, as in **d**. Depicted genes belong to the lists of genes characterizing the biological responses shown in **e**. (**c**,**e**) Number of genes (histograms) and –log *P* value (grey squares) of the enriched biological processes are plotted. *P* values

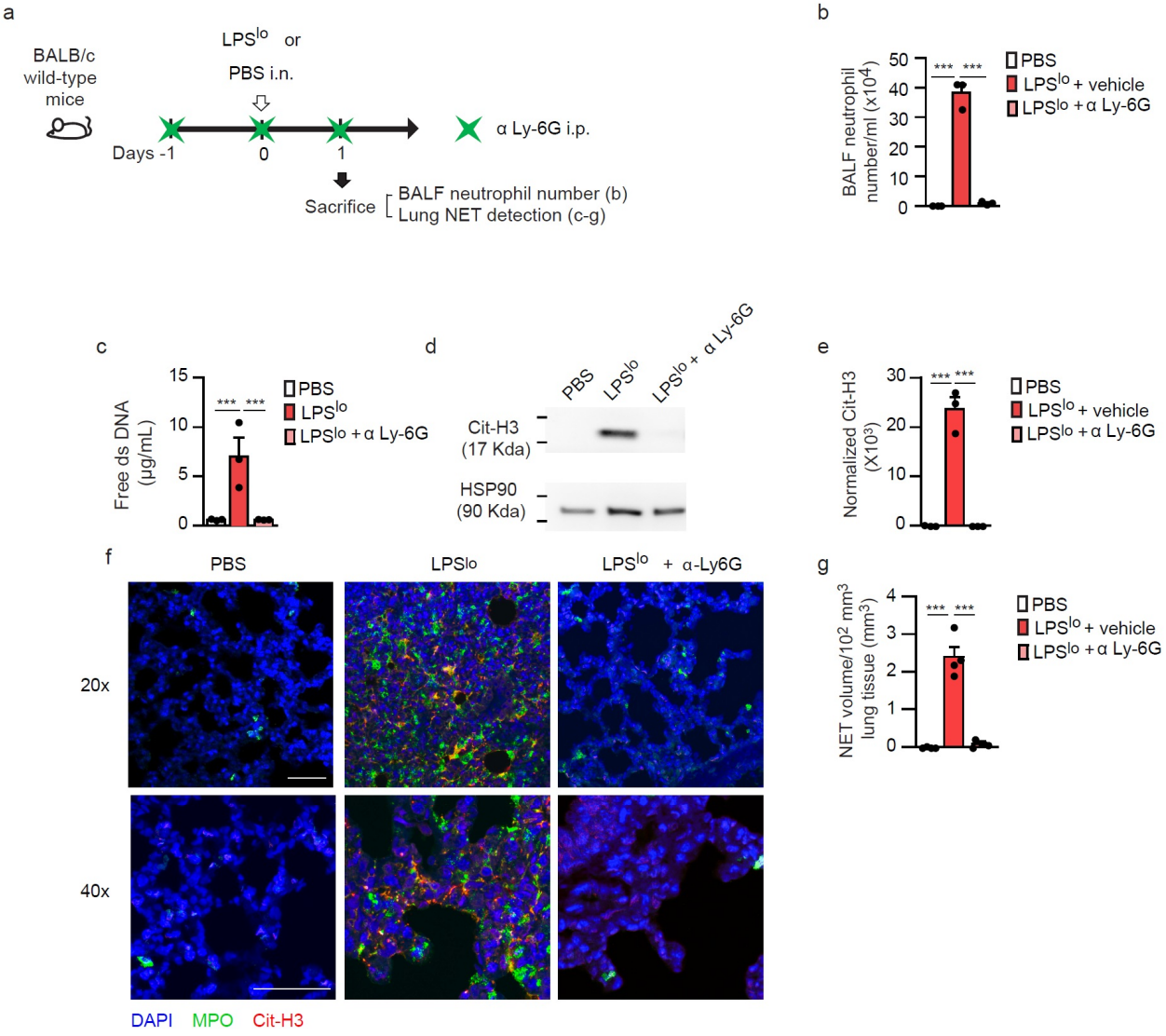
were calculated using a two-tailed Mann-Whitney U test with Benjamini-Hochberg False Discovery Rate (FDR) correction.


a
LPSlo or
LPShi or
PBS i.n.
Sort neutrophils
after 24 hours
PBS
CXCR4lo
CD49dlo
cells
LPSlo
CXCR4hi
CD49dhi
cells
LPShi
CXCR4lo
CD49dlo
cells
Lung neutrophil morphology (b-d)
NET detection ex vivo (e-g)
b
PBS
LPSlo
LPShi
c
Size (μm2)
150
100
50
0
**
***
PBS
LPSlo
LPShi
d
Nucleus/cytoplasm ratio
0.4
0.2
0
***
***
PBS
LPSlo
LPShi
e
DAPI
MPO
Cit-H3
Merged
PBS CXCR4lo CD49dlo cells
LPSlo CXCR4hi CD49dhi cells
LPShi CXCR4lo CD49dlo cells
f
PBS CXCR4lo CD49dlo cells
LPSlo CXCR4hi CD49dhi cells
LPShi CXCR4lo CD49dlo cells
DAPI MPO Cit-H3
g
NET volume per 10² neutrophils (mm³)
80
60
40
20
0
ns
***
***
PBS
LPSlo
LPShi

Supplementary Figure 4

LPS^{lo} neutrophils, unlike steady-state or LPS^{hi} neutrophils, are dedicated to form NETs ex vivo.

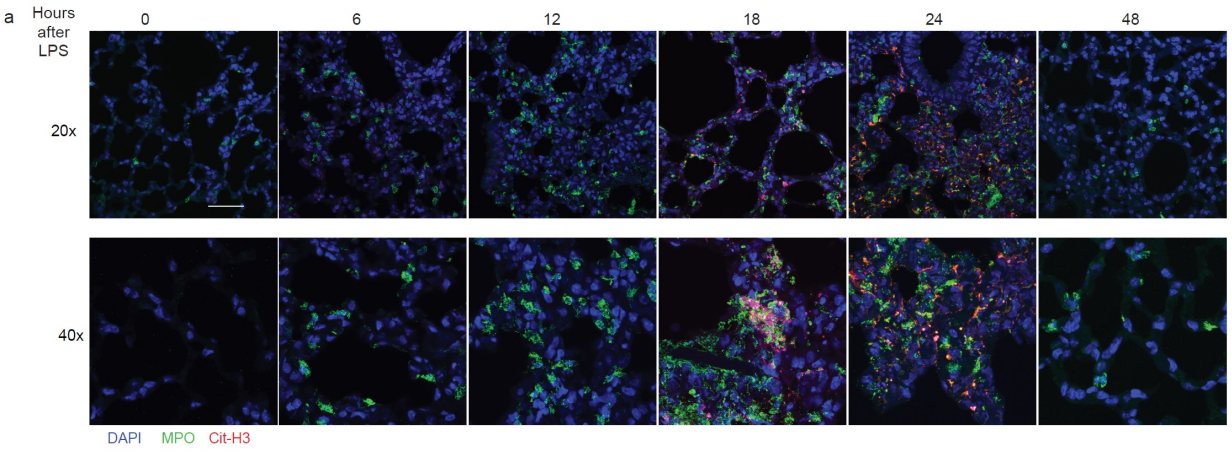
a, Experimental outline. **b**, Representative photographs of FACS-sorted CXCR4^{lo}CD49d^{lo}, CXCR4^{lo}CD49d^{lo} and CXCR4^{hi}CD49d^{hi} lung neutrophils from vehicle, LPS^{lo} and LPS^{hi} mice 24 h after treatment. **c**, Quantification of the size of neutrophils from mice as in **b**. **d**, Quantification of the nucleus/cytoplasm ratio of neutrophils from mice as in **b**. **e**,**f**, Representative high-resolution confocal microscopy pictures of Cit-H3^{+}MPO^{+}DAPI^{+} NETs released from ex vivo-cultured neutrophils as in **b**. **e**, Representative pictures of the individual and merged stainings, magnification 20x. **f**, Additional representative pictures of the merged stainings, magnification 10x. **g**, Quantification of NET volume in *ex vivo*-cultured neutrophils as in **b**. Data show mean + s.e.m., each symbol representing independent sorting experiments in which cells from 2–3 mice were pooled by group (**c**,**d**,**g**: n = 6,4 independent experiments, respectively). P values were calculated using a one-way ANOVA with Tukey's *post hoc* test. $^{**}P < 0.01$; $^{***}P < 0.001$. i.n., intranasal. ns, not significant. Scale bar = (**b**) 10 μm; (**e,f**) 50 μm.

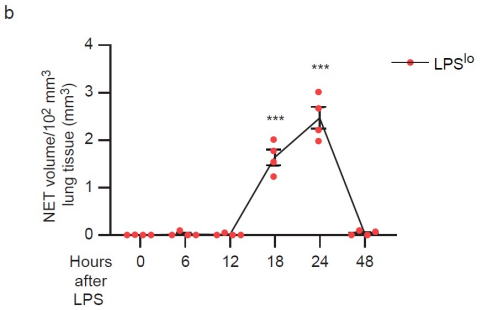


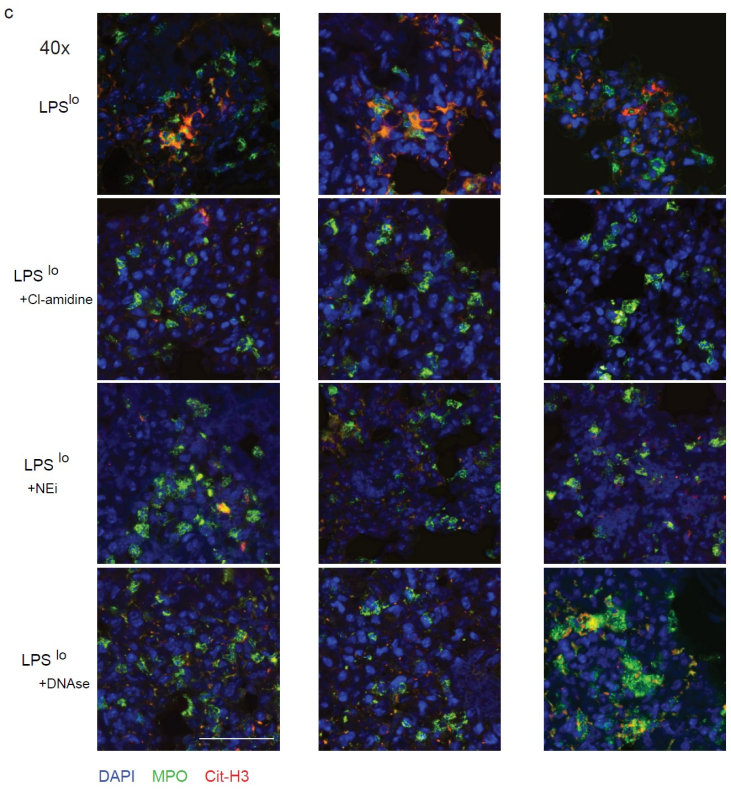
Supplementary Figure 5

NETs are not detected in LPS^{lo} mice treated with α-Ly-6G neutrophil-depleting antibodies

a, Experimental outline. **b**, Neutrophil cell counts in the broncho-alveolar lavage fluid (BALF) of vehicle and LPS^{lo} mice treated or not i.p. with α-Ly-6G antibodies one day before, at the time of and one day after LPS^{lo} exposure. **c**, Levels of extracellular dsDNA in the BALF of mice as in **b**. **d**, Representative blots of Cit-H3 and HSP90α (loading control) assessed by Western blot of lung protein extracts from mice as in **b**. **e**, Quantification of normalized Cit-H3 levels in lung protein extracts of mice as in **b**. **f**, Confocal microscopy stainings of Cit-H3^{+}MPO^{+} NETs on lung sections of mice as in **b**. Pictures shown are representative of one of >3 mice analyzed, each of them giving similar results. **g**, Quantification of NET volume in lung sections of mice as in **b**. (**b**,**c**,**e**,**g**) Data show mean + s.e.m., as well as individual mice, and (**b,c,e**) are representative of one of 3 independent experiments yielding similar results (**b**,**c**,**e**: *n* = 3 mice per group; g: *n* = 4 mice per group). *P* values were calculated using a one-way ANOVA with Tukey's *post hoc* test. ***$P < 0.001$. BALF, bronchoalveolar lavage fluid; i.p., intraperitoneal; ns, not significant. Scale bar = 50 μm.


a
Hours after LPS
0
6
12
18
24
48
20x
40x
DAPI MPO Cit-H3

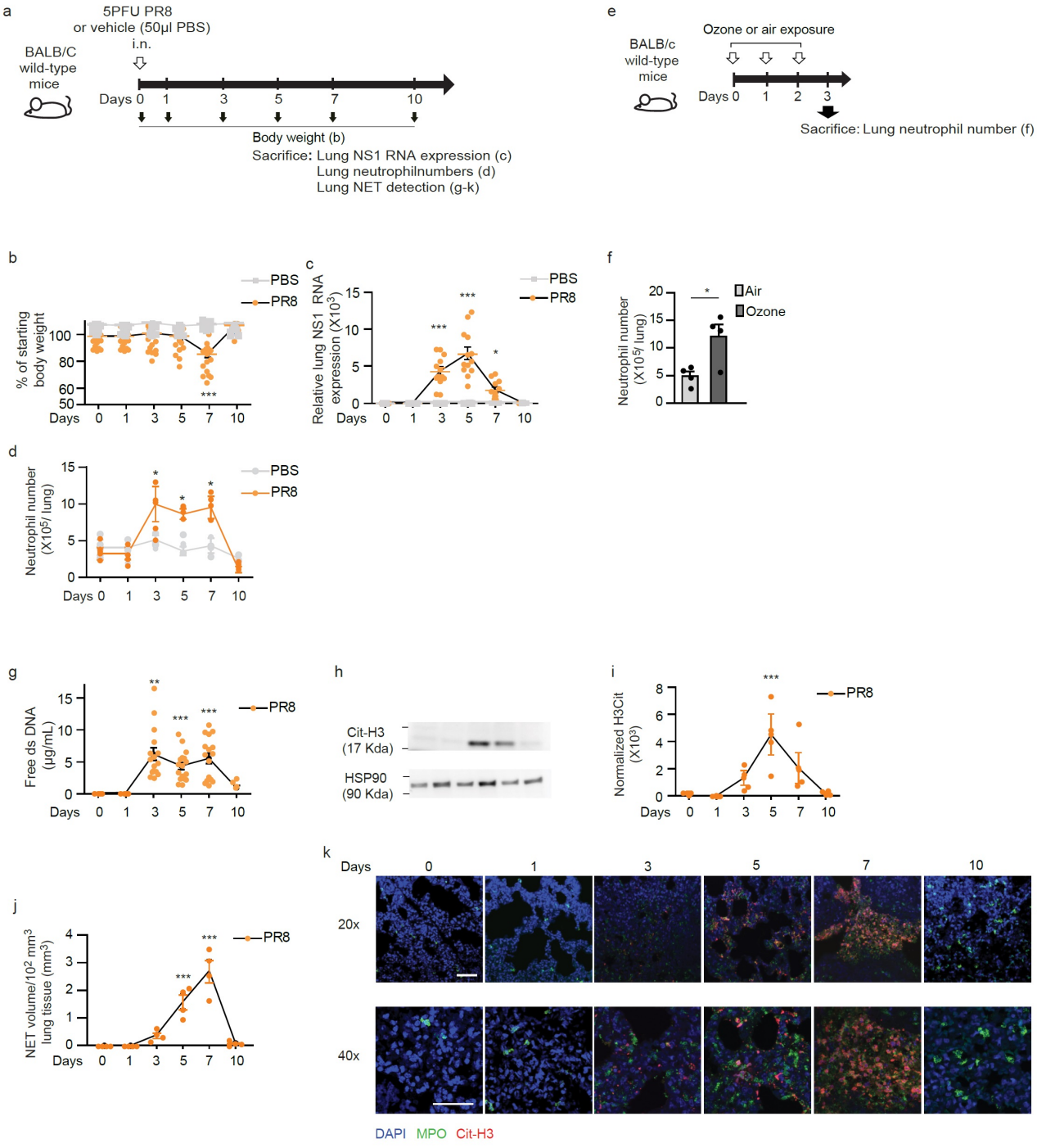

b
NET volume/10² mm³ lung tissue (mm³)
LPS^lo
***
***
Hours after LPS
0
6
12
18
24
48


c
40x
LPS^lo
LPS^lo +Cl-amidine
LPS^lo +NEi
LPS^lo +DNAse
DAPI MPO Cit-H3

Supplementary Figure 6

NETs appear in the lung 18 h after LPS^{lo} exposure and are impaired in lungs of LPS^{lo} mice treated with DNAse, Cl-amidine or NEi

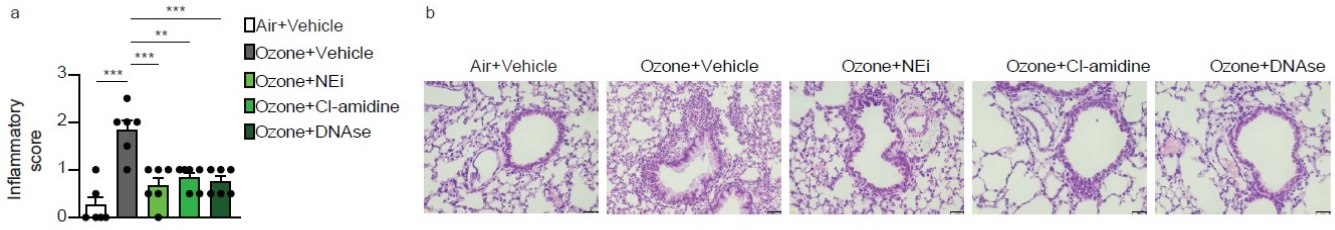
a, Confocal microscopy stainings of Cit-$H3^{+}MPO^{+}$ NETs on lung sections of mice 0, 6, 12, 18, 24 and 48 h after LPS^{lo} treatment. Pictures are representative of one of 4 mice analyzed, each of them giving similar results. **b,** Quantification of NET volume on lung sections of mice as in **a**. **c**, Confocal microscopy stainings of Cit-$H3^{+}MPO^{+}$ NETs on lung sections, assessed 24 h after LPS^{lo} in mice treated i.p. with DNAse one day before and at the time of LPS^{lo} treatment, or treated 4 times i.p. with NEi or Cl-amidine, every 12 h starting one day before LPS^{lo}. Pictures are representative of one of 5 mice analyzed, each of them giving similar results. Quantification of NET volume is shown in Fig. 5b. (**b**) Data show mean + s.e.m., as well as individual mice (n = 4 per time point). P values were calculated using a one-way ANOVA with Tukey's *post hoc* tests and compare the indicated time points with the baseline (hour 0). $^{***}P <$ 0.001. NEi, neutrophil elastase inhibitor. Scale bar = 50 μm.


a
5PFU PR8
or vehicle (50µl PBS)
i.n.
BALB/C
wild-type
mice
Days 0 1 3 5 7 10
Body weight (b)
Sacrifice: Lung NS1 RNA expression (c)
Lung neutrophilnumbers (d)
Lung NET detection (g-k)
e
Ozone or air exposure
BALB/c
wild-type
mice
Days 0 1 2 3
Sacrifice: Lung neutrophil number (f)
b
% of starting
body weight
PBS
PR8
Days 0 1 3 5 7 10
c
Relative lung NS1 RNA
expression (X10³)
f
Neutrophil number
(X10⁵/ lung)
Air
Ozone
d
Neutrophil number
(X10⁵/ lung)
g
Free ds DNA
(µg/mL)
h
Cit-H3
(17 Kda)
HSP90
(90 Kda)
i
Normalized H3Cit
(X10³)
j
NET volume/10² mm³
lung tissue (mm³)
k
Days 0 1 3 5 7 10
20x
40x
DAPI MPO Cit-H3

Supplementary Figure 7

NET-releasing neutrophils are recruited to the lungs on influenza virus PR8 infection and ozone exposure

a, Experimental outline for panels **b**–**d** and **g**–**k**. **b**, Body weight expressed as the % of body weight before influenza virus (H1N1 strain PR8) infection, assessed over time in PBS-injected and PR8-infected mice. **c**, Lung relative RNA expression of viral non-structural protein 1 (NS1) assessed by RT-qPCR over time in PBS-injected or PR8-infected mice. **d**, Absolute numbers of lung $CD45^{+}CD11b^{hi}Ly\text{-}6G^{hi}$ neutrophils assessed over time in PBS-injected or PR8-infected mice. **e**, Experimental outline for **f**. **f**, Absolute numbers of lung $CD45^{+}CD11b^{hi}Ly\text{-}6G^{hi}$ neutrophils assessed in air-exposed and ozone-exposed mice 1 d after the last ozone exposure. **g**, Levels of extracellular dsDNA in the BALF of mice following PR8 infection. **h**, Representative blots of Cit-H3 and HSP90α (loading control) assessed by Western blot of lung protein extracts of mice following PR8 infection. **i**, Quantification of normalized Cit-H3 levels in lung protein extracts of mice following PR8 infection. **j**, Quantification of NET volume in lung sections of mice following PR8 infection. **k**, Confocal microscopy stainings of $Cit\text{-}H3^{+}MPO^{+}$ NETs on lung sections of mice following PR8 infection. Pictures shown are representative of one of 4 mice analyzed, each of them giving similar results. (**b**,**c**) Data show mean +/– s.e.m. and are pooled from 4 independent experiments, each symbol representing individual mice, ([b] PBS: *n* = 20,20,20,18,19,20 at days 0,1,3,5,7,10, respectively; PR8: *n* = 20,20,20,18,20,10 at days 0,1,3,5,7,10, respectively; [c] PBS: *n* = 8 at each time point; PR8: *n* = 8,8,13,13,12,8 at days 0,1,3,5,7,10 respectively). (**d**,**f**) Data show mean (**d**) +/– or (**f**) + s.e.m. and are pooled from 2 independent experiments, each symbol representing individual mice (*n* = 3–4 mice per group). (**g**,**i**,**j**) Data show mean +/– s.e.m. and are pooled from 3–5 independent experiments, each symbol representing (**g**,**j**) individual mice (g: *n* = 9,7,16,17,16,7 at days 0,1,3,5,7,10, respectively; j: *n* = 4 mice per time point), or (**i**) independent experiments in which lungs from 3–5 mice were pooled by group (*n* = 4 independent experiments). *P* values were calculated using (**b**,**c**,**d**) a two-way ANOVA with Tukey's *post hoc* test and compare PBS *vs.* PR8 at the indicated time points, (**f**) a two-tailed unpaired Student's *t* test or (**g**,**i**,**j**) a one-way ANOVA with Tukey's *post hoc* test and compare the indicated time points with the baseline. $^{*}P<0.05$; $^{**}P < 0.01$; $^{***}P < 0.001$. BALF, bronchoalveolar lavage fluid; ns, not significant i.n., intranasal; PFU, plaque forming unit. Scale bar = 50 μm.



Supplementary Figure 8

Ozone-potentiated HDM-induced perivascular and peribronchial leukocyte infiltration is decreased upon treatment with NEi, Cl-Amidine or DNAse

a, Inflammatory score estimating perivascular and peribronchial inflammation, quantified from H&E-stained lung sections 3 d after the second HDM administration in vehicle-HDM and ozone-HDM mice treated daily for 4 d with DNAse i.p., starting the first day of ozone exposure, or treated every 12 h with NEi or Cl-amidine i.p., for the same duration as for DNAse. **b**, Representative H&E staining of lung sections of mice as in **a**. Pictures are representative of one of 6 mice analyzed, each of them giving comparable results. (**a**) Data show mean + s.e.m. and are pooled from 2 independent experiments (n = 6 mice per group). P values were calculated using a one-way ANOVA with Tukey's *post hoc* test. $^{**}P < 0.01$; $^{***}P < 0.001$. NEi, neutrophil elastase inhibitor. Scale bar = 32 μm.

nature research

Corresponding author(s): Thomas MARICHAL, Fabrice BUREAU

Last updated by author(s): Aug 12, 2019

Reporting Summary

Nature Research wishes to improve the reproducibility of the work that we publish. This form provides structure for consistency and transparency in reporting. For further information on Nature Research policies, see Authors & Referees and the Editorial Policy Checklist.

Statistics

For all statistical analyses, confirm that the following items are present in the figure legend, table legend, main text, or Methods section.

n/a	Confirmed	
☐	☒	The exact sample size (*n*) for each experimental group/condition, given as a discrete number and unit of measurement
☐	☒	A statement on whether measurements were taken from distinct samples or whether the same sample was measured repeatedly
☐	☒	The statistical test(s) used AND whether they are one- or two-sided *Only common tests should be described solely by name; describe more complex techniques in the Methods section.*
☒	☐	A description of all covariates tested
☐	☒	A description of any assumptions or corrections, such as tests of normality and adjustment for multiple comparisons
☐	☒	A full description of the statistical parameters including central tendency (e.g. means) or other basic estimates (e.g. regression coefficient) AND variation (e.g. standard deviation) or associated estimates of uncertainty (e.g. confidence intervals)
☐	☒	For null hypothesis testing, the test statistic (e.g. *F*, *t*, *r*) with confidence intervals, effect sizes, degrees of freedom and *P* value noted *Give P values as exact values whenever suitable.*
☒	☐	For Bayesian analysis, information on the choice of priors and Markov chain Monte Carlo settings
☒	☐	For hierarchical and complex designs, identification of the appropriate level for tests and full reporting of outcomes
☒	☐	Estimates of effect sizes (e.g. Cohen's *d*, Pearson's *r*), indicating how they were calculated

Our web collection on statistics for biologists contains articles on many of the points above.

Software and code

Policy information about availability of computer code

Data collection	Cell Ranger software (v1.2.0) (10x Genomics) was used to demultiplex Illumina BCL files to FASTQ files (cellranger mkfastq), to perform alignment (to mouse GRCm38/mm10 genome), filtering, UMI counting and to produce gene – barcode matrices (cellranger count).
Data analysis	Single cell analysis used R bioconductor (version 3.4.2.), and the R package Seurat (version 2.1.0). Statistical enrichment tests for GO biological processes were performed with PANTHER 13.1. Flow cytometry analysis were performed with FlowJo (version 10.1, Tree Star, Ashland, USA). Immunofluorescence images were acquired on a Zeiss LSM 880 Airyscan Elyra S.1. confocal microscope (Zeiss) and analyzed using the ImageJ (version 15.1n) and Imaris (version 7.5.2) softwares. Statistics: GraphPad Prism 6 for PC, R Bioconductor.

For manuscripts utilizing custom algorithms or software that are central to the research but not yet described in published literature, software must be made available to editors/reviewers. We strongly encourage code deposition in a community repository (e.g. GitHub). See the Nature Research guidelines for submitting code & software for further information.

Data

Policy information about availability of data

All manuscripts must include a data availability statement. This statement should provide the following information, where applicable:

- Accession codes, unique identifiers, or web links for publicly available datasets
- A list of figures that have associated raw data
- A description of any restrictions on data availability

The scRNA-seq data provided in this manuscript have been deposited in the ArrayExpress database at EMBL-EBI (https://www.ebi.ac.uk/arrayexpress/experiments/E-MTAB-6902) under accession number E-MTAB-6902. The figures that have associated raw data are the following: Fig. 2, Supplementary Figs. 2,3.

Field-specific reporting

Please select the one below that is the best fit for your research. If you are not sure, read the appropriate sections before making your selection.

☒ Life sciences ☐ Behavioural & social sciences ☐ Ecological, evolutionary & environmental sciences

For a reference copy of the document with all sections, see nature.com/documents/nr-reporting-summary-flat.pdf

Life sciences study design

All studies must disclose on these points even when the disclosure is negative.

Sample size	We assume that variance will be equal between experimental groups. We estimate that a difference will be biologically significant between two groups if a variation of at least 50% is observed between the mean of the two groups. If we want to compare two means of 1500 and 3000 with a standard deviation of 750 (example from the number of eosinophils in the bronchoalveolar lavage fluid of asthmatics and controls mice) , the results of power analysis for expecting effects show that for a power of 0.9 (and $\alpha<0.05$) in a t student test, the required sample size would be 3-5 animals. In most of the experiments, 3 to 10 mice/group was sufficient to identify differences between groups with at least 90% power and a 5% significance level.
Data exclusions	No data was excluded from the analyses.
Replication	For each experiment, each experimental group was composed of 3-5 mice constituting biological replicates. Each experiments have been repeated two to four times. All attempts at replication were successful and gave similar readout.
Randomization	Female age-matched BALB/c mice were randomly allocated into experimental groups.
Blinding	Blinding was only relevant for histological analysis of H&E and PAS stained-lung sections. All other conclusions were made based on quantitative parameters and statistical significance.

Reporting for specific materials, systems and methods

We require information from authors about some types of materials, experimental systems and methods used in many studies. Here, indicate whether each material, system or method listed is relevant to your study. If you are not sure if a list item applies to your research, read the appropriate section before selecting a response.

Materials & experimental systems

n/a	Involved in the study
☐	☒ Antibodies
☒	☐ Eukaryotic cell lines
☒	☐ Palaeontology
☐	☒ Animals and other organisms
☒	☐ Human research participants
☒	☐ Clinical data

Methods

n/a	Involved in the study
☒	☐ ChIP-seq
☐	☒ Flow cytometry
☒	☐ MRI-based neuroimaging

Antibodies

Antibodies used	Anti-mouse FITC-, and V500-conjugated anti-CD45.2 (clone 104, dilution 1/100, #561874, #562130), PE-conjugated anti-CD3 (clone 142-2C11, dilution 1/100, #553064), PE-conjugated anti-CD19 (clone 1D3, dilution 1/300, #553786), PE-conjugated anti-NK1.1 (clone pk136, dilution 1/300, # 553165), PE-conjugated anti-Siglec-F (clone E50-2440, dilution 1/500,#552126), PE-conjugated anit-Ly6G (clone 1A8, dilution 1/500, #551461), eFluor450- and PE-Cy7-conjugated anti-CD11b (clone M1/70, dilution 1/300, #560455, #561098), PE-Cy7-conjugated anti-Ly6G (clone 1A8, dilution 1/200, #560501), APC-Cy7-conjugated anti-CD11c (clone HL3, dilution 1/150, #561241), PE-CF594-conjugated anti-Ly6C (clone 49-44, dilution 1/200, #562728), FITC-conjugated anti-CD103 (clone M290, dilution 1/100, #557494) and PE-conjugated anti-Lamp-1 (CD107a) (clone 1D4B, dilution 1/100, #558661), Anti-mouse PE-conjugated anti-CXCR4 (clone 2B11, dilution 1/100, #561734) antibodies were purchased from BD biosciences. Anti-mouse PE-conjugated anti-CD49d (clone R1-2, dilution 1/100, #12-0492-81) antibodies were purchased from eBioscience. Anti-mouse PerCP-Cy5.5-conjugated anti-MHC-II (Ia-Ie) (clone M5/M4,15,2, dilution 1/1000, #107626) and BV421-conjugated anti-CD64 (clone X54-5/7.1, dilution 1/100, #139309) antibodies were purchased from Biolegend. Unconjugated Goat anti-myeloperoxydase (dilution 1/40, #AF3667) was purchased from R&D systems and unconjugated rabbit anti-histone H3 citrullinated (dilution 1/100, #ab5103) was purchased from abcam.
Validation	All the antibodies are from commercial sources and purhcased from BD pharmingen, Ebioscience, biolegend, R&D systems and abcam. The data sheets were provided by the manufacturer, in which the validation of antibodies for the specificity to the mouse antigen and for the usage for flow cytometry/western blot/confocal microscopy was confirmed. Statements about validation are found in manufacturer's website.

Animals and other organisms

Policy information about studies involving animals; ARRIVE guidelines recommended for reporting animal research

Laboratory animals	Mus musculus, BALB/c, female, 6 to 10 weeks
Wild animals	The study did not involve wild animals.
Field-collected samples	The study did not involve samples collected from the field.
Ethics oversight	All animal experiments described in this study were reviewed and approved by the Institutional Animal Care and Use Committee of the University of Liège. The "Guide for the Care and Use of Laboratory Animals", prepared by the Institute of Laboratory Animal Resources, National Research Council, and published by the National Academy Press, as well as European and local legislations, were followed carefully.

Note that full information on the approval of the study protocol must also be provided in the manuscript.

Flow Cytometry

Plots

Confirm that:

☒ The axis labels state the marker and fluorochrome used (e.g. CD4-FITC).

☒ The axis scales are clearly visible. Include numbers along axes only for bottom left plot of group (a 'group' is an analysis of identical markers).

☒ All plots are contour plots with outliers or pseudocolor plots.

☒ A numerical value for number of cells or percentage (with statistics) is provided.

Methodology

Sample preparation	To obtain single-lung-cell suspensions, lungs were perfused with 10 ml of PBS through the right ventricle, cut into small pieces, and digested for 1 h at 37°C in HBSS containing 1 mg/ml collagenase A (Roche) and 0.05 mg/ml DNase I (Roche). Blood was collected in an EDTA-containing tube (100 mM), and red blood cells were lysed with RBC lysis buffer (eBioscience). BM cells were isolated by flushing femurs with PBS.Staining reactions were performed at 4°C after incubation with 2.4G2 Fc receptor blocking antibodies to avoid non-specific binding. Anti-mouse Lamp-1 intracellular staining was performed using the Foxp3/Transcription factor Staining Buffer Set from eBiosciences according to the manufacturer's instructions. Briefly, after extracellular staining, cells were resuspended in 200 µl of Fix/Perm buffer for 45 minutes at 4°C in the dark and then washed with 200 µl of permeabilization buffer. Cells were then stained for intracellular protein in permeabilization buffer for 35-40 minutes.
Instrument	Cell phenotyping and sorting were performed on a FACSCANTO II and a FACSARIA III (BD Biosciences), respectively.
Software	FlowJo (version 10.1, Tree Star, Ashland, USA)
Cell population abundance	Purity was between 90 and 95% and was determined by flow cytometry after sorting.
Gating strategy	Lung dendritic cells (DCs) were selected as CD45+CD3e-CD19-Siglec-F-Ly6G-NK1.1-MHCII+CD11c+ cells and were then subdivided into CD11b-CD103+, CD11b+Ly-6C- and CD11b+Ly-6C+ subsets ; lung neutrophils were selected as SSChighCD45.2 +CD11bhighLy-6Ghigh cells. Bone marrow dendritic cells (BMDCs) were selected as MHC-II+CD11c+ cells and further divided between CD11b+Ly-6C+ and CD11b+Ly-6C- subsets.

☒ Tick this box to confirm that a figure exemplifying the gating strategy is provided in the Supplementary Information.